



THE UNIVERSITY *of* EDINBURGH

## Edinburgh Research Explorer

### **Synergistic melanoma cell death mediated by inhibition of both MCL1 and BCL2 in high-risk tumors driven by NF1/PTEN loss**

**Citation for published version:**

He, S, Zimmerman, MW, Layden, HM, Berezovskaya, A, Etchin, J, Martel, MW, Thurston, G, Jing, C-B, van Rooijen, E, Kaufman, CK, Rodig, SJ, Zon, LI, Patton, EE, Mansour, MR & Look, AT 2021, 'Synergistic melanoma cell death mediated by inhibition of both MCL1 and BCL2 in high-risk tumors driven by NF1/PTEN loss', *Oncogene*. <https://doi.org/10.1038/s41388-021-01926-y>

**Digital Object Identifier (DOI):**

[10.1038/s41388-021-01926-y](https://doi.org/10.1038/s41388-021-01926-y)

**Link:**

[Link to publication record in Edinburgh Research Explorer](#)

**Document Version:**

Peer reviewed version

**Published In:**

Oncogene

**General rights**

Copyright for the publications made accessible via the Edinburgh Research Explorer is retained by the author(s) and / or other copyright owners and it is a condition of accessing these publications that users recognise and abide by the legal requirements associated with these rights.

**Take down policy**

The University of Edinburgh has made every reasonable effort to ensure that Edinburgh Research Explorer content complies with UK legislation. If you believe that the public display of this file breaches copyright please contact [openaccess@ed.ac.uk](mailto:openaccess@ed.ac.uk) providing details, and we will remove access to the work immediately and investigate your claim.



1 **Synergistic melanoma cell death mediated by inhibition of both MCL1 and BCL2 in high-**  
2 **risk tumors driven by NF1/PTEN loss**

3

4 Shuning He<sup>1,\*</sup>, Mark W. Zimmerman<sup>1</sup>, Hillary M. Layden<sup>1</sup>, Alla Berezovskaya<sup>1</sup>, Julia Etchin<sup>1</sup>,  
5 Megan W. Martel<sup>1</sup>, Grace Thurston<sup>1</sup>, Chang-Bin Jing<sup>1</sup>, Ellen van Rooijen<sup>2</sup>, Charles K. Kaufman<sup>2</sup>,  
6 Scott J. Rodig<sup>3</sup>, Leonard I. Zon<sup>2</sup>, E. Elizabeth Patton<sup>4</sup>, Marc R. Mansour<sup>1,5,\*</sup>, and A. Thomas  
7 Look<sup>1,\*</sup>

8

9 <sup>1</sup>Department of Pediatric Oncology, Dana-Farber Cancer Institute, Harvard Medical School,  
10 Boston MA, 02115, USA.

11 <sup>2</sup>Stem Cell Program and Division of Hematology/Oncology, Children's Hospital Boston, Howard  
12 Hughes Medical Institute, Boston, MA, 02115, USA.

13 <sup>3</sup>Department of Pathology, Brigham and Women's Hospital, Boston, MA, 02115, USA.

14 <sup>4</sup>MRC Human Genetics Unit, MRC Institute of Genetics and Molecular Medicine, University of  
15 Edinburgh, Crewe Road South, Edinburgh, EH4 2XR, UK.

16 <sup>5</sup>Department of Hematology, UCL Cancer Institute, University College London, WC1E 6BT, UK.

17

18 \*To whom correspondence should be addressed: shuning\_he@dfci.harvard.edu (S.H.),  
19 m.mansour@ucl.ac.uk (M.R.M), Thomas\_Look@dfci.harvard.edu (A.T.L.)

20

21 **Competing interests:** The authors have declared that no conflict of interest exists.

22

23    **Abstract**

24    Melanomas driven by loss of the NF1 tumor suppressor have a high risk of treatment failure and  
25    effective therapies have not been developed. Here we show that loss-of-function mutations of *nfl*  
26    and *pten* result in aggressive melanomas in zebrafish, representing the first animal model of NF1-  
27    mutant melanomas harboring PTEN loss. MEK or PI3K inhibitors show little activity when given  
28    alone due to cross-talk between the pathways, and high toxicity when given together. The mTOR  
29    inhibitors, sirolimus, everolimus and temsirolimus, were the most active single agents tested,  
30    potently induced tumor-suppressive autophagy, but not apoptosis. Because addition of the BCL2  
31    inhibitor venetoclax resulted in compensatory upregulation of MCL1, we established a three-drug  
32    combination composed of sirolimus, venetoclax and the MCL1 inhibitor S63845. This well-  
33    tolerated drug combination potently and synergistically induces apoptosis in both zebrafish and  
34    human NF1/PTEN-deficient melanoma cells, providing preclinical evidence justifying an early-  
35    stage clinical trial in patients with NF1/PTEN-deficient melanoma.

36

## 37    **Introduction**

38    Cutaneous melanoma accounts for the vast majority of skin cancer-related deaths. More than  
39    100,000 newly diagnosed cases of melanoma are projected in the United States for 2020 together  
40    with ~6,800 melanoma-related deaths<sup>1</sup>. The Cancer Genome Atlas (TCGA) classified cutaneous  
41    melanomas into four molecular subtypes: *BRAF*-mutant (47.5%), *RAS*-mutant (29%), *NFI*-mutant  
42    (9%), and triple-wild-type (14.5%)<sup>2</sup>. The *NFI*-mutant category refers to cases lacking either  
43    *BRAF* or *RAS* mutations, whereas *NFI* mutations can also arise as a mechanism of resistance to  
44    RAF/MEK-targeted therapies in *BRAF*-mutated melanoma<sup>3,4</sup>. Thus, *NFI* mutations have been  
45    reported in 13-17% of cutaneous melanomas overall<sup>2,5,6</sup>.

46        The *NFI* gene encodes neurofibromin, a 2818-amino-acid protein whose GTPase-activating  
47    protein-related domain negatively regulates RAS signaling by catalyzing the hydrolysis of RAS-  
48    GTP into RAS-GDP. Thus, one consequence of *NFI*-loss is the aberrant activation of RAS  
49    signaling<sup>7</sup>. In primary melanoma patient biopsies, *NFI* mutations were not correlated with hot-  
50    spot *BRAF* mutations, a finding consistent with a redundant role for these two types of mutations  
51    in activating RAS-MAPK signaling.

52        Recent efforts to develop improved targeted therapies for melanoma have mainly focused  
53    on the *BRAF*-mutant subtype, leaving a paucity of treatment options for patients with *NFI*-mutant  
54    melanomas. It is unlikely that the FDA-approved *BRAF*-mutant-specific inhibitors will be  
55    beneficial against *BRAF*-wild-type, *NFI*-mutant melanomas. Moreover, analysis of multiple  
56    clinical trials indicate that the *NFI*-mutant subtype has the worst outcome among all metastatic  
57    melanomas<sup>8</sup>. Clearly, a better understanding of the molecular pathogenesis of *NFI*-mutant  
58    melanomas is needed to improve the design and hence the outcome of treatments for this subtype  
59    of melanoma.

60        A major impediment to the development of targeted therapies for patients with *NFI*-mutant  
61    melanomas has been the lack of suitable animal models. For example, both the *BRAF*-mutant and

62 *RAS*-mutant subtypes of melanoma have been successfully modeled in mice<sup>9</sup> and zebrafish<sup>10</sup> by  
63 combining the melanoma-associated mutations in these genes with mutation or loss of *p53* or  
64 *Cdkn2a*, which are both typically inactivated in human melanoma<sup>2,11</sup>. However, *Nf1*-loss was not  
65 sufficient to induce melanoma tumorigenesis in mice<sup>3,12</sup> or zebrafish<sup>13</sup>, either alone or in  
66 combination with *p53*-loss. As the NF1-mutant melanomas often harbor a high mutation load<sup>14,15</sup>,  
67 we reasoned that genetic or epigenetic alterations affecting genes other than *p53* and *Cdkn2a* are  
68 likely required in combination with *NF1*-loss to initiate melanoma transformation *in vivo*.  
69 Because a significant subset of human *NF1*-mutant melanomas harbor genetic alterations leading  
70 to activation of the PI3K-AKT-mTOR pathway<sup>2,6</sup>, we hypothesized that targeting this pathway  
71 through inactivation of *ptena/ptenb* would drive melanomagenesis in *nfl/p53*-mutant zebrafish.

72

## 73 Results

74

### 75 Loss-of-function mutations of *nf1* and *pten* cooperate to drive melanomagenesis in *p53*- 76 deficient zebrafish.

77 We previously reported the development of *nf1a*<sup>+/-</sup>;*nf1b*<sup>-/-</sup> zebrafish lines with loss of three  
78 of the four functional alleles of *nf1*<sup>13</sup>. These animals develop spontaneous malignant peripheral  
79 nerve sheath tumors (MPNSTs) with low penetrance, but not melanomas, beginning at the age of  
80 1.5 years, indicating that *nf1*-loss alone is not sufficient to drive melanomagenesis  
81 (Supplementary Figure S1). When we bred the *nf1a*<sup>+/-</sup>;*nf1b*<sup>-/-</sup> line into a *p53*-deficient  
82 (*p53*<sup>M214K/M214K</sup>) background, the compound mutant fish developed MPNSTs or high-grade  
83 gliomas<sup>13</sup>. Although rare spontaneous melanomas were also detected, they had a very low  
84 penetrance (<2%) over the course of 40 weeks (Supplementary Figure S1). Because human *NF1*-  
85 mutant melanomas often harbor gain-of-function alterations in the PI3K signaling pathway,  
86 including mutational inactivation of PTEN or overexpression of AKT3<sup>2,6</sup>, we introduced *pten*  
87 loss-of-function mutations into *nf1a*<sup>+/-</sup>;*nf1b*<sup>-/-</sup>;*p53*<sup>M214K/M214K</sup> zebrafish by crossing with a  
88 previously established *ptena*<sup>+/-</sup>;*ptenb*<sup>-/-</sup> line<sup>16,17</sup>. We then incrossed *nf1a*<sup>+/-</sup>;*nf1b*<sup>+/-</sup>;*ptena*<sup>+/-</sup>;*ptenb*<sup>+/-</sup>  
89 ;*p53*<sup>+/M214K</sup> fish and monitored the offspring for spontaneous tumor development every 2 weeks  
90 starting at 5 weeks of age. Very aggressive melanotic tumors began to appear in these fish at 7  
91 weeks of age, with a penetrance of 80% by 20 weeks (Figures 1a-e). Histopathologic study of the  
92 melanotic tumors revealed a dense, cellular neoplasm in which a subset of the neoplastic cells  
93 produced pigment, with an overall histology pathognomonic of malignant melanoma (Figures 1b-  
94 d). Thus, activation of the PI3K pathway appears to be a critical requirement for melanomas to  
95 develop, in this case in concert with loss of *NF1* and *p53*.

96 Melanomas arising in the *nf1/pten/p53*-mutant background were highly invasive into  
97 underlying musculature (Figures 1b-d), and developed much earlier than melanomas in either the

98 *Tg(mitf:BRAF<sup>V600E</sup>);p53<sup>M214K/M214K</sup>* or *Tg(mitf:NRAS<sup>Q61K</sup>);p53<sup>M214K/M214K</sup>* zebrafish<sup>18-21</sup>. MPNSTs  
 99 and glioblastomas appear in the *nf1/p53* background after 30 weeks of age, while melanomas  
 100 develop starting at 5 weeks of age in the *nf1/pten/p53* background and grow so rapidly that fish  
 101 usually need to be sacrificed for humane reasons before 30 weeks of age, so melanomas are the  
 102 only tumor-type observed in the *nf1/pten/p53* background. Importantly, these spontaneous  
 103 melanomas arose exclusively in fish that were homozygous null for both *nf1b* and *ptenb*,  
 104 heterozygous for *nf1a* and *ptena* mutant alleles, and either heterozygous or homozygous for  
 105 *p53<sup>M214K</sup>* (Figures 1 and S2). DNA PCR from melanoma tumors and adjacent normal tissue  
 106 showed that the wild-type allele of *nf1a* and *ptena* is retained by the tumor cells (Supplementary  
 107 Figure S3). The *nf1a<sup>+/-</sup>;nf1b<sup>-/-</sup>;ptena<sup>+/-</sup>;ptenb<sup>-/-</sup>;p53<sup>M214K/M214K</sup>* tumors (designated “*nf1/pten*-  
 108 mutant melanomas”) developed at random sites across the surface of the fish (Figure 1a). The  
 109 pigmented melanoma cells were highly invasive, infiltrating skeletal muscle adjacent to every  
 110 tumor examined for histology (Figures 1b-d). Hence, retention of only one allele of both *nf1* and  
 111 *pten* in a p53-mutant background drives the development of highly invasive malignant melanoma  
 112 in our zebrafish model.

113

#### 114 **The *nf1/pten*-mutant melanomas lack *braf/nras* hot-spot mutations.**

115 Since 80% of human cutaneous melanomas harbor activating hot-spot mutations in either  
 116 *BRAF* or *NRAS* (e.g., *BRAFV600*, *NRASG12* or *NRASQ61*)<sup>2</sup>, we examined the *nf1/pten*-mutant  
 117 zebrafish melanomas for spontaneous mutations at equivalent sites in the zebrafish orthologues  
 118 (Supplementary Figure S4). Sequencing of eight tumors revealed only wild-type alleles of these  
 119 two genes in each tumor (Supplementary Figure S5). Hence, similar to the *NF1*-mutant class of  
 120 human cutaneous melanomas<sup>2</sup>, the loss of *nf1* is sufficient to provide RAS pathway activation,  
 121 and zebrafish melanomas in this background do not contain *braf/nras* hot-spot mutations.

122

123 ***nf1/pten*-mutant melanomas exhibit aberrant activation of the RAS and PI3K pathways and**  
124 **are highly proliferative.**

125 Since NF1 and PTEN are well-established negative regulators of RAS and PI3K  
126 signaling<sup>7,22</sup>, respectively, we postulated that the *nf1/pten*-mutant melanomas would exhibit  
127 activation of effector pathways downstream of *RAS* and *PI3K*. Indeed, we detected high levels of  
128 phosphorylated ERK (pERK), phosphorylated AKT (pAKT) and phosphorylated S6 ribosomal  
129 protein (pS6, an mTOR downstream effector) by immunohistochemistry (IHC) in the *nf1/pten*-  
130 mutant melanomas (Figure 1f), indicating hyperactivation of both RAS and PI3K pathways.  
131 Because these pathways drive proliferation, we next analyzed the proliferative capacity of  
132 *nf1/pten*-mutant melanomas, observing high levels of expression of proliferating cell nuclear  
133 antigen (PCNA) in 45% of tumor cell nuclei but not the adjacent normal tissue (Figure 1f),  
134 indicating a high tumor proliferative rate. Apoptotic cells were not observed in these melanomas,  
135 as indicated by the lack of detectable cleaved caspase-3 (Figure 1f). Hence, combined activation  
136 of the RAS and PI3K pathways, a high proliferative rate and the lack of apoptosis likely account  
137 for the rapid onset and high growth rate of *nf1/pten*-mutant melanomas.

138

139 ***nf1/pten*-mutant melanomas can be serially transplanted into immunodeficient recipients.**

140 To assess the transplantation potential of our melanoma model, we isolated *nf1/pten*-  
141 mutant melanoma cells and transplanted them intraperitoneally into the optically clear  
142 immunodeficient *rag2*<sup>E450fs</sup>(*casper*) zebrafish<sup>23</sup> (designated “*rag2*<sup>-/-</sup>”). Robust engraftment was  
143 observed at the site of injection. All recipient fish demonstrated rapidly growing melanotic tumor  
144 masses within 2 weeks (Figure 1g). Because of the invasive properties of the primary *nf1/pten*-  
145 mutant melanomas (Figure 1), we also tested the feasibility of their intramuscular transplantation  
146 into *rag2*<sup>-/-</sup> zebrafish, where the tumor cells not only expanded within muscle, but also invaded  
147 neighboring tissues such as the ventral fin (Supplementary Figure S6). By contrast, non-



transformed melanocytes (derived from normal pigmented melanocytes within the skin stripes) from *nf1a*<sup>+/-</sup>;*nf1b*<sup>-/-</sup>;*ptena*<sup>+/-</sup>;*ptenb*<sup>-/-</sup>;*p53*<sup>M214K/M214K</sup> zebrafish failed to engraft in *rag2*<sup>-/-</sup> zebrafish. Furthermore, although the melanomas arising from the *Tg(mitf:BRAF<sup>V600E</sup>);p53<sup>M214K/M214K</sup>* zebrafish<sup>24</sup> can be serially transplanted into *rag2*<sup>-/-</sup> zebrafish, their post-transplantation growth rates were much slower, highlighting the extraordinarily high growth rate *in vivo* of the *nf1/pten*-mutant melanomas.

154

**MEK and PI3K inhibitors lack efficacy against *nf1/pten*-mutant melanomas *in vivo*.**

Human *NF1*-mutant melanomas have the worst outcome among all metastatic melanomas<sup>8</sup>, and *PTEN*-mutant melanomas are known to be resistant to T-cell mediated immunotherapy such as the immune checkpoint inhibitor<sup>25</sup>. Thus, there is a clear need for effective small molecule inhibitors to overcome the aggressive growth properties of *NF1/PTEN*-mutant melanoma. Because targeting the RAS-MEK-ERK and PI3K-PTEN-AKT-mTOR signaling pathways might logically affect the growth of *nf1/pten*-mutant melanomas, we first transplanted these melanoma cells into 3-week-old *rag2*<sup>-/-</sup> zebrafish and treated the recipients with MEK (trametinib or cobimetinib) or pan-PI3K (buparlisib or apitolisib) inhibitors. The *nf1/pten*-mutant melanoma cells grew rapidly in DMSO-treated recipients and progressed from an inoculum of 500 cells to readily detectable pigmented tumors at 4-8 days post-transplantation (Figure 2a). Single-agent treatment with either MEK or PI3K inhibitors from days 2-8 post-transplantation at each of their maximum tolerated dosages (MTDs; Supplementary Figure S7a) did not affect the growth of tumors (Figures 2b and S7b). Even when tumor-bearing recipient fish were treated with a combination of trametinib and buparlisib at their MTDs (Supplementary Figure S7a), tumor growth was only transiently inhibited during treatment, followed by rapid regrowth after drug removal, resulting in the lack of improvement in overall survival (Figure 2d).

172

173 **Inhibition of mTOR suppresses the growth of *nfl/pten*-mutant melanomas *in vivo*.**

174 To broaden the coverage of candidate pathway inhibitors, we next tested a panel of  
175 antitumor drugs targeting the RAS-MEK-ERK and receptor tyrosine kinase-PI3K-AKT-mTOR  
176 pathways in our *nfl/pten*-mutant melanoma model by assessing tumor cell growth and overall  
177 survival of recipient *rag2*<sup>-/-</sup> fish after 6 days of treatment (Figures 2, S8 and S9). Among the 14  
178 tested drugs, each at their MTD, only the rapamycin family of mTOR inhibitors (rapalogs)  
179 showed selective activity against *nfl/pten*-mutant melanoma *in vivo* as single agents.  
180 Interestingly, four different mTOR kinase inhibitors did not show activity against *nfl/pten*-mutant  
181 melanomas at their MTD (Supplementary Figure S9). During the 6-day treatment course,  
182 sirolimus (rapamycin) clearly suppressed the appearance of detectable tumors, and its inhibition  
183 of tumor growth persisted for 1 to 2 weeks post-treatment, in marked contrast to the rapid tumor  
184 regrowth in fish treated with MEK and PI3K inhibitors (Figures 2c, 2e, 3 and S10). We also  
185 treated *nfl/pten*-mutant melanomas with everolimus and temsirolimus, two FDA-approved  
186 analogs of sirolimus. The three rapalogs showed similar abilities to durably inhibit melanoma cell  
187 growth (Figures 2c and e), which uniformly translated to improved overall survival, indicating  
188 that rapalogs may provide a useful treatment option for these melanomas *in vivo*.

189 Primary *nfl/pten*-mutant tumors are invariably melanotic, but after serial transplantation,  
190 the tumor cells often become amelanotic<sup>26</sup>. In order to track the melanoma cells using EGFP  
191 instead of melanin, we bred the *sox10*:EGFP fluorescent zebrafish line into our *nfl/pten*-mutant  
192 line to aid in visualization of the transplanted melanoma cells, as they expressed high levels of the  
193 neural crest progenitor marker *sox10* (Supplementary Figure S11)<sup>24</sup>. When transplanted into 3-  
194 week-old *rag2*<sup>-/-</sup> zebrafish and treated for 6 days with multiple different inhibitors, the EGFP-  
195 expressing amelanotic cells responded poorly to single-agent treatment with either trametinib or  
196 buparlisib, had only temporary responses to the trametinib-buparlisib combination, but showed  
197 more durable responses to sirolimus and temsirolimus (Supplementary Figure S12). Thus, the

198 amelanotic melanoma cells appear to respond in a similar fashion to the melanotic melanoma  
199 cells, reinforcing the dependence of both subtypes of melanoma on mTOR signaling for  
200 malignant cell growth *in vivo*.

201

202 **Cell growth in *nfl/pten*-mutant melanomas depends on mTOR signaling.**

203       The RAS-MEK-MAPK and PI3K-AKT-mTOR pathways negatively regulate each other,  
204 such that a drug-induced blockade of one pathway results in increased activity of the other<sup>27,28</sup>. To  
205 test whether these drugs act on the expected pathways in inhibitor-treated *nfl/pten*-mutant  
206 melanomas, we analyzed treated tumors by IHC, observing that treatment with the MEK inhibitor  
207 trametinib leads to a reduction in pERK levels (Figures 4a and b), as expected; while levels of  
208 pAKT and pS6 are increased (Figures 4a, c and d), reflecting the loss of RAS-MEK-MAPK-  
209 mediated cross-inhibition of PI3K-AKT-mTOR signaling<sup>28</sup>. Similarly, treatment with the PI3K  
210 inhibitor buparlisib led to a reduction in pAKT and pS6 levels, with loss of RAS-MEK-MAPK-  
211 mediated cross-inhibition, resulting in increased pERK levels (Figures 4a-d). This concomitant  
212 upregulation of an alternative pathway explains why neither buparlisib nor trametinib alone  
213 inhibited tumor-cell proliferation (Figures 4a and e). The trametinib-buparlisib combination  
214 readily inhibited both the RAS and PI3K pathways, leading to a significant, though modest,  
215 decrease in tumor-cell proliferation (Figure 4). Thus, these two pathways appear to function  
216 redundantly in driving the proliferation of *nfl/pten*-mutant melanomas. Interestingly, 2 days of  
217 sirolimus treatment resulted in undetectable levels of pS6 staining (Figures 4a and d), reflecting  
218 mTOR inhibition with transient increase and then sustained loss of pERK levels (Figures 4a, 4b  
219 and 5) and suppression of proliferation (Figure 4). Thus, the sustained compensatory  
220 upregulation of the ERK pathway induced by buparlisib was not evident when mTOR-mediated  
221 phosphorylation was specifically inhibited by sirolimus.

222 To assess the durability of pathway suppression by inhibitor treatment, we treated *nf1/pten*-  
223 mutant-melanoma recipients with the inhibitors for 6 days, then analyzed the tumors after 4 days  
224 in the absence of the drugs. Sirolimus led to sustained reductions in pERK, pAKT, pS6, and  
225 PCNA levels at 4 days post-treatment (Figures 5a-c), as part of a cytoprotective autophagy stress  
226 response (Figure 6a). By contrast, the initial signaling and antiproliferative effects of the  
227 trametinib-buparlisib combination (Figure 4) were short-lived, as 4 days after drug removal, the  
228 pERK, pAKT, pS6 and PCNA levels were returning to normal (Figure 5). Similar to sirolimus,  
229 temsirolimus also induced durable inhibition of pS6 and sustained suppression of pERK, pAKT  
230 and tumor proliferation (Supplementary Figure S13). Thus, in contrast to combined inhibition of  
231 PI3K and MEK, mTOR inhibition alone leads to the sustained suppression of RAS and PI3K  
232 pathways and tumor cell growth in transplanted melanomas.

233

234 **Co-inhibition of BCL2 and MCL1 synergizes with sirolimus to cause apoptotic cell death**  
235 ***nf1/pten*-mutant melanomas *in vivo***

236 It is important to emphasize that while either sirolimus or temsirolimus can induce prolonged  
237 proliferative arrest based on the absence of PCNA staining, we did not detect cleaved caspase 3 in  
238 treated tumor cells (Figures 4a, 5a and S13), indicating that neither agent is cytotoxic as a single  
239 agent. To query further the proliferative arrest induced by these rapalogs, we studied the  
240 autophagy marker LC3 by IHC. This analysis revealed autophagy not only of the tumor cells by  
241 LC3 staining, but also striking levels of autophagy in the brain and liver of the sirolimus-treated  
242 animals (Figure 6a). The absence of a cytotoxic effect and initiation of autophagy as a cell  
243 survival mechanism would likely limit the therapeutic potential of rapalogs in *nf1/pten*-mutant  
244 melanomas. Thus, we analyzed a panel of antitumor drugs to identify those with the potential to  
245 synergize with sirolimus by inducing apoptosis, thus converting “cytostatic autophagy” to  
246 “cytotoxic autophagy”<sup>29</sup>. This evaluation included MEK inhibitors trametinib and cobimetinib,

247 the PI3K inhibitors buparlisib and apitolisib, the pan-RAF inhibitor sorafenib, the PARP inhibitor  
248 olaparib, the autophagy inhibitor chloroquine, and inhibitors of the BCL2 family of pro-survival  
249 proteins including sabutoclax, obatoclax, venetoclax and S63845 (MTD determination see  
250 Supplementary Figure S14).

251 As shown in Supplementary Figure S15, none of the drugs delayed tumor progression when  
252 given alone to 3-week-old fish bearing *nf1/pten*-mutant melanomas, and only sirolimus in  
253 combination with venetoclax showed overall survival benefit compared to sirolimus alone. In  
254 particular, the autophagy inhibitor chloroquine markedly delayed tumor progression when  
255 combined with sirolimus, presumably by blocking the ability of the autophagosomes to fuse with  
256 lysosomes, thus preventing both tumor and normal cells from accessing the nutrients sequestered  
257 in the autophagosome<sup>30-32</sup>. However, its use with sirolimus caused massive post-treatment death  
258 of the recipient fish as early as 4 days after drug administration, presumably due to autophagy of  
259 normal tissues such as liver (Figures 6 and S15). Thus, we sought to identify drugs that would  
260 modify the autophagy response not directly as in the case of chloroquine but selectively by  
261 promoting apoptosis.

262 Pro-survival members of the BCL2 family of proteins are required for the survival of cells  
263 undergoing autophagy<sup>33</sup>, with tumor cells typically showing greater dependence on these pro-  
264 survival effects because of their higher-than-normal expression of BH3-only initiators of  
265 apoptosis, leading to an increased propensity to undergo apoptosis through a mechanism called  
266 “apoptotic priming”<sup>34</sup>. Thus, since pro-survival BCL2 family proteins are essential in the high-  
267 stress environment induced by sirolimus, their inhibition would be expected to induce tumor cells  
268 to undergo apoptosis before normal cells<sup>35-38</sup>. Therefore, inhibitors of pro-survival BCL2 family  
269 proteins should have a therapeutic index based on synergy with the effects of sirolimus in targeted  
270 therapy for “primed” NF1/PTEN-mutant tumor cells, while sparing normal tissues.

271 To test this hypothesis, we focused on two inhibitors, venetoclax (inhibiting BCL2)<sup>39</sup> and  
272 S63845 (inhibiting MCL1)<sup>40</sup>. Interestingly, although venetoclax alone had no effect on tumor  
273 growth at a dose of 7.5  $\mu$ M, its combination with 10  $\mu$ M sirolimus significantly delayed tumor  
274 progression (Figures 6b and c). Similarly, S63845 alone did not affect tumor growth at a dose of 5  
275  $\mu$ M, but in combination with 10  $\mu$ M sirolimus, it augmented the growth suppressive effects of  
276 sirolimus (Figures 6d and e).

277 It is known that each member of the pro-survival BCL2 family proteins, including BCL2 and  
278 MCL1, can bind and sequester BH3-only proteins independently and thereby prevent these BH3-  
279 only proteins from inducing apoptosis by activating BAX and BAK<sup>39</sup>. We previously discovered  
280 in vivo synergistic anti-leukemia activity of venetoclax and S63845, as each drug causes marked  
281 compensatory upregulation of MCL1 and BCL2 protein levels when used as single agent in  
282 zebrafish<sup>41</sup>. Hence, we reasoned that co-inhibition of BCL2 and MCL1 in *nfl/pten*-mutant  
283 melanoma cells might produce an even greater synergistic antitumor effect than observed with  
284 either inhibitor given individually with sirolimus. Indeed, when we combined 7.5  $\mu$ M venetoclax  
285 and 2.5  $\mu$ M S63845 with 10  $\mu$ M sirolimus, we observed greatly enhanced growth suppression of  
286 *nfl/pten*-mutant melanoma cells (Figures 6f and g). To determine the basis for this boosted  
287 effect, we analyzed the contributions of these three agents to tumor cell proliferation and  
288 apoptosis. 7.5  $\mu$ M venetoclax and 2.5  $\mu$ M S63845 had no effect on proliferation or apoptosis,  
289 while 10  $\mu$ M sirolimus significantly inhibited proliferation but failed to induce apoptosis (Figures  
290 6h and i). In combination, however, the three drugs effectively inhibited proliferation, and  
291 dramatically increased levels of apoptosis (Figures 6h and i). Importantly, the fish tolerated this  
292 drug combination without noticeable toxicity. Thus, our results indicate that tumor cells  
293 sensitized by sirolimus become more dependent than normal cells on BCL2 and MCL1 for  
294 sustained survival, thus increasing their susceptibility to apoptosis in the absence of these key pro-  
295 survival proteins.

296

297 **Co-inhibition of BCL2 and MCL1 synergizes with sirolimus to induce apoptosis in human**  
298 ***NF1/PTEN*-deficient melanoma cells**

299 To validate the efficacy of our three-drug combination, we turned to studies using human  
300 *NF1/PTEN*-deficient melanoma cells. For this purpose, we first evaluated the expression level of  
301 neurofibromin and PTEN in a panel of human melanoma cell lines and identified one cell line,  
302 WM-3246, that lacked detectable expression of either neurofibromin or PTEN (Figure 7a). Then,  
303 using WM-3246 cells, we tested the effects of sirolimus, venetoclax and S63845 on the viability  
304 of *NF1/PTEN*-deficient melanoma cells. As a single agent, sirolimus induced only modest levels  
305 of cytostatic growth suppression at concentrations >50 nM (Figures 7b-d). Venetoclax did not  
306 produce effects on WM-3246 cell growth at concentrations up to 250 nM, whereas S63845  
307 suppressed cell growth in a dose-dependent manner at doses >5 nM (Figures 7b-c). The greatest  
308 impact on cell growth was evident when sirolimus was tested in combination with venetoclax and  
309 S63845 (Figures 7c-d); synergy was obtained by isobologram analysis over a range of drug  
310 concentrations (Figure 7e), indicating that these cells depend on both BCL2 and MCL1, as well as  
311 on mTOR signaling, for cell growth and survival. Western blot analysis showed compensatory  
312 upregulation of MCL1 in cells treated with venetoclax (Figure 7f), confirming the molecular basis  
313 for the synergy between S63845 and venetoclax in sirolimus-treated WM-3246 cells.  
314 Furthermore, cleaved caspase 3 in WM-3246 cells treated with the three-drug combination but not  
315 with sirolimus alone (Figure 7g), validating the induction of apoptosis by co-inhibition of BCL2  
316 and MCL1 in sirolimus-sensitized *NF1/PTEN*-deficient human melanoma cells.

317 We also tested the three-drug combination identified in our *NF1/PTEN*-mutant melanoma  
318 model in BRAF-mutant melanomas with PTEN-mutations, because BRAF activation by mutation  
319 is more prevalent than biallelic inactivating mutations of NF1. Although each of these drugs  
320 demonstrated little or no activity as single agents, the three-drug combination showed significant

321 activity against the BRAF-mutant melanoma cells harboring PTEN-mutation (Supplementary  
322 Figure S16). Furthermore, the venetoclax-S63845 combination potentiated melanoma cell killing  
323 caused by the BRAFV600E inhibitor darafenib in BRAF-mutant melanoma cells (Supplementary  
324 Figure S16), suggesting that co-inhibition of BCL2 and MCL1 as a strategy to enhance the  
325 induction of apoptosis has broad utility as a means to potentiate the activity of targeted therapies  
326 in disseminated human melanomas.

327



328 **Discussion**

329 Loss-of-function mutations of the *NF1* tumor suppressor in human melanoma cells were first  
330 identified by us and others in the early 1990s<sup>42,43</sup>. The TCGA program subsequently undertook a  
331 multiplatform characterization of cutaneous melanoma samples at the DNA, RNA and protein  
332 levels, in which *NF1*-mutant melanoma emerged as an important subtype within a genomic  
333 classification framework<sup>2</sup>. Although highly useful as a means to identify cooperative molecular  
334 aberrations that might serve as druggable targets or predictive biomarkers, this genomic approach  
335 did not suggest a therapeutic strategy for tumors linked to *NF1*-loss. Using a zebrafish  
336 experimental system that models human NF1-mutant melanomas, we show that activation of both  
337 the RAS and PI3K pathways in a background of *pten*-loss is required to initiate melanomas in  
338 *nf1*-deficient animals. However, the RAS and PI3K pathways function redundantly in tumor  
339 maintenance, due to compensatory upregulation of either pathway when the other is inhibited  
340 (Figures 4 and 5). Even simultaneous inhibition of both pathways only transiently inhibited the  
341 growth of *nf1/pten*-mutant melanomas, such that the overall survival of tumor-bearing fish was  
342 unaffected (Figures 2, S7 and S10). This result contrasts with findings in basal-like breast cancer  
343 cell lines, in which the combination of MEK and PI3K inhibitors produced cytotoxic antitumor  
344 effects<sup>44</sup>.

345 Given the superiority of sirolimus in suppressing the growth of transplanted *nf1/pten*-mutant  
346 melanomas while inducing autophagy in normal tissues, we faced a major challenge: to identify  
347 drugs that could selectively cause apoptosis in sirolimus-sensitized melanoma cells. Such studies  
348 require an animal model that allows one to simultaneously assess both antitumor effects and  
349 toxicity to normal tissues, a criterion that was readily met by our zebrafish model. Indeed, while  
350 the antitumor response of *nf1/pten*-mutant melanomas to the combination of sirolimus and  
351 chloroquine initially appeared promising, the treated fish died due to toxicity to normal tissues  
352 (Supplementary Figure S15), illustrating the importance of analyzing this drug combination in an

353 in vivo model system. By contrast, the combination of sirolimus with inhibitors of the anti-  
354 apoptotic proteins BCL2 (venetoclax) and MCL1 (S63845) was both well tolerated by normal  
355 tissues and highly active in inducing apoptosis in tumor cells (Figures 6, 7 and S15). This  
356 selectivity apparently results from the fact that the malignant cells are “primed” to undergo  
357 apoptosis, while normal cells do not harbor the same levels of upregulation of BH3-only death  
358 proteins and can survive and maintain mitochondrial integrity despite the simultaneous inhibition  
359 of two major pro-survival proteins.

360 Our results underscore the advantages of using a reliable in vivo preclinical model to analyze  
361 the effects of simultaneously inhibiting multiple pathways with small-molecule drugs. Given its  
362 greater efficiency and lower costs compared to murine models, our zebrafish experimental system  
363 appears ideal for pursuing additional classes of pathway inhibitors in *NF1/PTEN*-mutant  
364 melanomas, as single agents and in combination, to define their clinical translational potential.  
365 Thus, the three-drug combination of sirolimus, venetoclax and S63845 is well tolerated at  
366 effective dosages in vivo and shows activity against human as well as zebrafish NF1/PTEN-  
367 deficient melanoma cells, providing preclinical evidence justifying an early stage clinical trial in  
368 patients with melanomas of this high-risk genomic subtype. Notably, the three-drug combination  
369 identified in our NF1/PTEN-mutant melanoma model also showed anti-melanoma activity in  
370 BRAF-mutant melanoma cells harboring PTEN-mutation (Supplementary Figure S16).  
371 Furthermore, the venetoclax-S63845 combination potentiated melanoma cell killing caused by the  
372 BRAFV600E inhibitor darafenib in BRAF-mutant melanoma cells (Supplementary Figure S16).  
373 Thus the potentiation of apoptosis induced by co-inhibition of BCL2 and MCL1 is a strategy with  
374 wide applicability to enhance the anti-melanoma activity by targeted therapies in malignant  
375 melanoma.

376

377 **Materials and Methods**

379 **Zebrafish**

380 Zebrafish experiments and animal husbandry were performed in accordance with Dana-Farber  
381 Cancer Institute IACUC-approved protocol #02-107.

383 **Melanoma tumor watch**

384 *nf1a*<sup>+/-</sup>; *nf1b*<sup>+/-</sup>; *ptena*<sup>+/-</sup>; *ptenb*<sup>+/-</sup>; *p53*<sup>+/*M214K*</sup> mutant zebrafish were incrossed, and offspring were  
385 monitored every week, starting at 3 weeks, for hyperpigmented cell masses indicative of  
386 melanoma tumors. Once a hyperpigmented cell mass was identified, the individual fish was  
387 separated and carefully monitored weekly for at least 3 weeks for tumor progression. Only fish  
388 with expanding hyperpigmented cell masses were scored as tumor fish and analyzed further by  
389 H&E staining and immunohistochemical assays. All fish were genotyped for *nf1a*, *nf1b*, *ptena*,  
390 *ptenb* and *p53* at the age of 6 weeks. The exact sample size (n) for each experimental group is  
391 indicated in the figures.

393 **Tumor cell transplantation**

394 *rag2*<sup>*E450fs*</sup>(*casper*) (*rag2*<sup>-/-</sup>) zebrafish were anaesthetized with 0.003% tricaine (Sigma-Aldrich, St.  
395 Louis, MO) and positioned on a 10-cm Petri dish coated with 1% agarose. Primary and serially-  
396 passaged tumors derived from *nf1a*<sup>+/-</sup>; *nf1b*<sup>-/-</sup>; *ptena*<sup>+/-</sup>; *ptenb*<sup>-/-</sup>; *p53*<sup>*M214K* /*M214K*</sup> and *nf1a*<sup>+/-</sup>; *nf1b*<sup>-/-</sup>  
397 ; *ptena*<sup>+/-</sup>; *ptenb*<sup>-/-</sup>; *p53*<sup>*M214K* /*M214K*</sup>; *Tg(sox10:EGFP)* zebrafish lines were excised from tumor-  
398 bearing fish and mechanically dissociated with a razor blade in 0.9X PBS + 5% FBS (Life  
399 Technologies, Carlsbad, CA) at room temperature. Collected cell suspension was filtered through  
400 a 40-μm cell strainer (Falcon, Corning, NY) and resuspended in 0.9X PBS + 5% FBS. For the  
401 intraperitoneal and intramuscular transplantation into 3- to 4-month-old adult *rag2*<sup>-/-</sup> fish, a

26s/2”/2 Hamilton 80300 syringe (Hamilton, Reno, NV) was used<sup>23</sup>. For the intraperitoneal transplantation into 3-week-old juvenile *rag2*<sup>-/-</sup> fish, cell suspensions were loaded into borosilicate glass capillary needles (1 mm o.d. × 0.78 mm i.d.; Harvard Apparatus, Holliston, MA), and the injections were performed with a Pneumatic Picopump and a manipulator (WPI, Sarasota, FL) <sup>45</sup>.

**Cell culture**

Melanoma cell lines Mewo, WM-3246, WM-3622, WM-3629, WM-3670 and WM-3918 were purchased from Rockland (Rockland Immunochemicals Inc, Limerick, PA), and maintained in Dulbecco's modified Eagle's medium supplemented with 10% FBS, L-glutamine, and penicillin/streptomycin. Melanoma cell lines COLO829 and C32 were purchased from ATCC (ATCC, Manassas, VA) and maintained according to the provided Culture Methods. HEK-293T cells were purchased from ATCC, and maintained in Dulbecco's modified Eagle's medium supplemented with 10% FBS, L-glutamine, and penicillin/streptomycin. Jurkart cells were maintained in RPMI-1640 medium supplemented with 10% FBS, L-glutamine, and penicillin/streptomycin. The identity of cell lines used in this study was verified by short tandem repeat analysis using the PowerPlex 1.2 system (Promega). The cell lines were tested for mycoplasma contamination using MycoAlert Mycoplasma Detection Kits (Lonza).

**Statistical analysis**

Statistical analysis was performed with Prism 5 software (GraphPad). Kaplan-Meier methods and the log-rank test were applied to assess the rate of tumor growth in Figure 1 and S1, and tumor progression in Figures 2, 6, S7, S8, S9, S10 and S15. The quantitative data in Figures 3, 4, 5 and S12 are reported as median values. A Mann-Whitney test with confidence intervals of 95% was used for the analyses in Figures 3, 4, 5, 6 and S12.

427 **References and Notes**

428 1 Siegel, R. L., Miller, K. D. & Jemal, A. Cancer statistics, 2020. *CA: A Cancer Journal for*  
429 *Clinicians* **70**, 7-30, doi:10.3322/caac.21590 (2020).

430 2 Akbani, R. *et al.* Genomic Classification of Cutaneous Melanoma. *Cell* **161**, 1681-1696,  
431 doi:<http://dx.doi.org/10.1016/j.cell.2015.05.044> (2015).

432 3 Maertens, O. *et al.* Elucidating Distinct Roles for NF1 in Melanomagenesis. *Cancer*  
433 *Discovery* **3**, 338-349, doi:10.1158/2159-8290.cd-12-0313 (2013).

434 4 Whittaker, S. R. *et al.* A Genome-Scale RNA Interference Screen Implicates NF1 Loss in  
435 Resistance to RAF Inhibition. *Cancer Discovery* **3**, 350-362, doi:10.1158/2159-8290.cd-  
436 12-0470 (2013).

437 5 Krauthammer, M. *et al.* Exome sequencing identifies recurrent mutations in NF1 and  
438 RASopathy genes in sun-exposed melanomas. *Nat Genet* **47**, 996-1002,  
439 doi:10.1038/ng.3361  
440 <http://www.nature.com/ng/journal/v47/n9/abs/ng.3361.html#supplementary-information> (2015).

441 6 Hayward, N. K. *et al.* Whole-genome landscapes of major melanoma subtypes. *Nature*  
442 **545**, 175-180, doi:10.1038/nature22071 (2017).

443 7 Maertens, O. & Cichowski, K. An expanding role for RAS GTPase activating proteins  
444 (RAS GAPs) in cancer. *Advances in Biological Regulation* **55**, 1-14,  
445 doi:<http://dx.doi.org/10.1016/j.jbior.2014.04.002> (2014).

446 8 Cirenajwis, H. *et al.* NF1-mutated melanoma tumors harbor distinct clinical and biological  
447 characteristics. *Molecular oncology* **11**, 438-451, doi:10.1002/1878-0261.12050 (2017).

448 9 Kuzu, O. F., Nguyen, F. D., Noory, M. A. & Sharma, A. Current State of Animal (Mouse)  
449 Modeling in Melanoma Research. *Cancer growth and metastasis* **8**, 81-94,  
450 doi:10.4137/cgm.s21214 (2015).

451 10 Kaufman, C. K. Zebrafish Melanoma. *Advances in experimental medicine and biology*  
452 **916**, 439-450, doi:10.1007/978-3-319-30654-4\_19 (2016).

453 11 Hodis, E. *et al.* A Landscape of Driver Mutations in Melanoma. *Cell* **150**, 251-263,  
454 doi:<http://dx.doi.org/10.1016/j.cell.2012.06.024> (2012).

455 12 De Raedt, T. *et al.* PRC2 loss amplifies Ras-driven transcription and confers sensitivity to  
456 BRD4-based therapies. *Nature* **514**, 247-251, doi:10.1038/nature13561  
457 [http://www.nature.com/nature/journal/v514/n7521/abs/nature13561.html#supplementary-](http://www.nature.com/nature/journal/v514/n7521/abs/nature13561.html#supplementary-information)  
458 [information](http://www.nature.com/nature/journal/v514/n7521/abs/nature13561.html#supplementary-information) (2014).

459 13 Shin, J. *et al.* Zebrafish neurofibromatosis type 1 genes have redundant functions in  
460 tumorigenesis and embryonic development. *Disease Models & Mechanisms* **5**, 881-894,  
461 doi:10.1242/dmm.009779 (2012).

462 14 Garman, B. *et al.* Genetic and Genomic Characterization of 462 Melanoma Patient-  
463 Derived Xenografts, Tumor Biopsies, and Cell Lines. *Cell reports* **21**, 1936-1952,  
464 doi:10.1016/j.celrep.2017.10.052 (2017).

465 15 Mar, V. J. *et al.* BRAF/NRAS wild-type melanomas have a high mutation load correlating  
466 with histologic and molecular signatures of UV damage. *Clinical cancer research : an*  
467 *official journal of the American Association for Cancer Research* **19**, 4589-4598,  
468 doi:10.1158/1078-0432.ccr-13-0398 (2013).

469 16 Gutierrez, A. *et al.* Pten mediates Myc oncogene dependence in a conditional zebrafish  
470 model of T cell acute lymphoblastic leukemia. *The Journal of Experimental Medicine* **208**,  
471 1595-1603, doi:10.1084/jem.20101691 (2011).

472 17 Faucherre, A., Taylor, G. S., Overvoorde, J., Dixon, J. E. & Hertog, J. d. Zebrafish pten  
473 genes have overlapping and non-redundant functions in tumorigenesis and embryonic  
474 development. *Oncogene* **27**, 1079-1086,  
475 doi:<http://www.nature.com/onc/journal/v27/n8/supinfo/1210730s1.html> (2007).

- Patton, E. *et al.* BRAF mutations are sufficient to promote nevi formation and cooperate with p53 in the genesis of melanoma. *Curr Biol* **15**, 249-254 (2005).
- Dovey, M., White, R. M. & Zon, L. I. Oncogenic NRAS Cooperates with p53 Loss to Generate Melanoma in Zebrafish. *Zebrafish* **6**, 397-404, doi:10.1089/zeb.2009.0606 (2009).
- Ceol, C. J. *et al.* The histone methyltransferase SETDB1 is recurrently amplified in melanoma and accelerates its onset. *Nature* **471**, 513-517, doi:<http://www.nature.com/nature/journal/v471/n7339/abs/10.1038-nature09806-unlocked.html#supplementary-information> (2011).
- Lister, J. A. *et al.* A conditional zebrafish MITF mutation reveals MITF levels are critical for melanoma promotion vs. regression in vivo. *The Journal of investigative dermatology* **134**, 133-140, doi:10.1038/jid.2013.293 (2014).
- Cully, M., You, H., Levine, A. J. & Mak, T. W. Beyond PTEN mutations: the PI3K pathway as an integrator of multiple inputs during tumorigenesis. *Nat Rev Cancer* **6**, 184-192 (2006).
- Tang, Q. *et al.* Imaging tumour cell heterogeneity following cell transplantation into optically clear immune-deficient zebrafish. *Nat Commun* **7**, doi:10.1038/ncomms10358 (2016).
- Kaufman, C. K. *et al.* A zebrafish melanoma model reveals emergence of neural crest identity during melanoma initiation. *Science* **351**, doi:10.1126/science.aad2197 (2016).
- Peng, W. *et al.* Loss of PTEN Promotes Resistance to T Cell-Mediated Immunotherapy. *Cancer Discov* **6**, 202-216, doi:10.1158/2159-8290.cd-15-0283 (2016).
- Chen, K. G. *et al.* Influence of melanosome dynamics on melanoma drug sensitivity. *J Natl Cancer Inst* **101**, 1259-1271, doi:10.1093/jnci/djp259 (2009).
- Yang, S., Xiao, X., Meng, X. & Leslie, K. K. A mechanism for synergy with combined mTOR and PI3 kinase inhibitors. *PLoS One* **6**, e26343, doi:10.1371/journal.pone.0026343 (2011).
- Mendoza, M. C., Er, E. E. & Blenis, J. The Ras-ERK and PI3K-mTOR pathways: cross-talk and compensation. *Trends in Biochemical Sciences* **36**, 320-328, doi:<http://dx.doi.org/10.1016/j.tibs.2011.03.006> (2011).
- Sharma, K., Le, N., Alotaibi, M. & Gewirtz, D. A. Cytotoxic autophagy in cancer therapy. *International journal of molecular sciences* **15**, 10034-10051, doi:10.3390/ijms150610034 (2014).
- Kaneko, M. *et al.* Temsirolimus and chloroquine cooperatively exhibit a potent antitumor effect against colorectal cancer cells. *Journal of cancer research and clinical oncology* **140**, 769-781, doi:10.1007/s00432-014-1628-0 (2014).
- Rangwala, R. *et al.* Combined MTOR and autophagy inhibition: phase I trial of hydroxychloroquine and temsirolimus in patients with advanced solid tumors and melanoma. *Autophagy* **10**, 1391-1402, doi:10.4161/auto.29119 (2014).
- Avniel-Polak, S. *et al.* Abrogation of Autophagy by Chloroquine Alone or in Combination with mTOR Inhibitors Induces Apoptosis in Neuroendocrine Tumor Cells. *Neuroendocrinology* **103**, 724-737, doi:10.1159/000442589 (2016).
- Macintosh, R. L. & Ryan, K. M. Autophagy in tumour cell death. *Seminars in cancer biology* **23**, 344-351, doi:10.1016/j.semcancer.2013.05.006 (2013).
- Potter, D. S. & Letai, A. To Prime, or Not to Prime: That Is the Question. *Cold Spring Harbor symposia on quantitative biology* **81**, 131-140, doi:10.1101/sqb.2016.81.030841 (2016).
- McGill, G. G. *et al.* Bcl2 regulation by the melanocyte master regulator Mitf modulates lineage survival and melanoma cell viability. *Cell* **109**, 707-718 (2002).

- 36 Mohana-Kumaran, N., Hill, D. S., Allen, J. D. & Haass, N. K. Targeting the intrinsic apoptosis pathway as a strategy for melanoma therapy. *Pigment cell & melanoma research* **27**, 525-539, doi:10.1111/pcmr.12242 (2014).
- 37 Lam, L. T. *et al.* A microRNA screen to identify modulators of sensitivity to BCL2 inhibitor ABT-263 (navitoclax). *Molecular cancer therapeutics* **9**, 2943-2950, doi:10.1158/1535-7163.mct-10-0427 (2010).
- 38 Mukherjee, N., Schwan, J. V., Fujita, M., Norris, D. A. & Shellman, Y. G. Alternative Treatments For Melanoma: Targeting BCL-2 Family Members to De-Bulk and Kill Cancer Stem Cells. *The Journal of investigative dermatology* **135**, 2155-2161, doi:10.1038/jid.2015.145 (2015).
- 39 Levenson, J. D. *et al.* Found in Translation: How Preclinical Research Is Guiding the Clinical Development of the BCL2-Selective Inhibitor Venetoclax. *Cancer Discov* **7**, 1376-1393, doi:10.1158/2159-8290.cd-17-0797 (2017).
- 40 Kotschy, A. *et al.* The MCL1 inhibitor S63845 is tolerable and effective in diverse cancer models. *Nature* **538**, 477-482, doi:10.1038/nature19830 (2016).
- 41 Li, Z., He, S. & Look, A. T. The MCL1-specific inhibitor S63845 acts synergistically with venetoclax/ABT-199 to induce apoptosis in T-cell acute lymphoblastic leukemia cells. *Leukemia* **33**, 262-266, doi:10.1038/s41375-018-0201-2 (2019).
- 42 Andersen, L. B. *et al.* Mutations in the neurofibromatosis 1 gene in sporadic malignant melanoma cell lines. *Nat Genet* **3**, 118-121 (1993).
- 43 Johnson, M. R., Look, A. T., DeClue, J. E., Valentine, M. B. & Lowy, D. R. Inactivation of the NF1 gene in human melanoma and neuroblastoma cell lines without impaired regulation of GTP.Ras. *Proceedings of the National Academy of Sciences* **90**, 5539-5543 (1993).
- 44 Hoeflich, K. P. *et al.* *In vivo* Antitumor Activity of MEK and Phosphatidylinositol 3-Kinase Inhibitors in Basal-Like Breast Cancer Models. *Clinical Cancer Research* **15**, 4649-4664, doi:10.1158/1078-0432.ccr-09-0317 (2009).
- 45 He, S. *et al.* Neutrophil-mediated experimental metastasis is enhanced by VEGFR inhibition in a zebrafish xenograft model. *The Journal of Pathology* **227**, 431-445, doi:10.1002/path.4013 (2012).

## Acknowledgments

We would like to thank John Gilbert for critical review of the manuscript and editorial suggestions; Kassandra Bacon and Daniel DeBiasi for zebrafish husbandry; Jeoren den Hertog, Alejandro Gutierrez and David M. Langenau for providing zebrafish lines; Yi Zhou and Andrew Hong for stimulating suggestions; Christine L. Unitt, Benjamin Ferland and Dana-Farber/Harvard Cancer Center Research Pathology Core for technical support. This study was funded by Melanoma Research Alliance award #509233.

565 **Figures and Tables**

566

567 **Figure 1: *nf1a*<sup>+/-</sup>;*nf1b*<sup>-/-</sup>;*ptena*<sup>+/-</sup>;*ptenb*<sup>-/-</sup>;*p53*<sup>M214K/M214K</sup> zebrafish spontaneously develop**  
568 **melanomas with rapid growth.**

569 (a) Representative 16-week-old *nf1a*<sup>+/-</sup>;*nf1b*<sup>-/-</sup>;*ptena*<sup>+/-</sup>;*ptenb*<sup>-/-</sup>;*p53*<sup>M214K/M214K</sup> zebrafish with one  
570 spontaneous melanoma (indicated by arrow). (b) Hematoxylin and eosin (H&E) staining of the  
571 melanoma tumor shown in panel a (5x magnification, scale bar = 200 μm). (c) Melanoma tumor  
572 cells from the black box in panel B, magnified 100X. (d) Melanoma tumor cells that have invaded  
573 into the dorsal muscle from the white box in panel B, magnified 100X. (e) Cumulative frequency  
574 of spontaneous melanomas arising in zebrafish with the indicated genotypes (generated by the  
575 inbreeding of the *nf1a*<sup>+/-</sup>;*nf1b*<sup>-/-</sup>;*ptena*<sup>+/-</sup>;*ptenb*<sup>-/-</sup>;*p53*<sup>M214K/M214K</sup> line, *p* < 0.0001, log-rank test). (f)  
576 Immunohistochemical analysis of melanoma tumor sections using antibodies to detect  
577 phosphorylated ERK1/2 (pERK), phosphorylated AKT (pAKT), phosphorylated S6 (pS6),  
578 proliferating cell nuclear antigen (PCNA) and cleaved caspase 3 (CC3) (63x magnification, scale  
579 bar = 20μm). The percentage of PCNA+ cells was determined by manually counting positive and  
580 negative melanoma cells in one representative high-power field (150 to 200 cells per field) within  
581 three independent tumor samples. (g) Pigmented *nf1/pten*-mutant melanoma cells were  
582 transplanted intraperitoneally into adult *rag2*<sup>-/-</sup> Casper zebrafish. The implanted melanoma cells  
583 (left panel, arrow) grew rapidly into secondary tumors (within 2 weeks; right panel).

584

585 **Figure 2: mTOR inhibitors achieve a durable antitumor effect in *nf1/pten*-mutant**  
586 **melanoma.**

587 (a) Schematic of the melanoma tumor transplantation assay. (b, c) Transplanted *nf1/pten*-mutant  
588 melanoma tumor cells were monitored daily in 3-week-old *rag2*<sup>-/-</sup> recipient zebrafish treated with  
589 DMSO (CTR; n=12), 80 nM trametinib (n=11), 2 μM buparlisib (n=11), or the combination of 80



590 nM trametinib and 2  $\mu$ M buparlisib (n=12) for 6 days. Kaplan-Meier curves for progression-free  
591 survival (PFS, panel b) and overall survival (OS, panel c) are shown. Statistical analyses were  
592 performed by log-rank test, comparing drug-treated with DMSO-treated zebrafish. (d, e)  
593 Transplanted *nf1/pten*-mutant melanoma tumor cells were monitored daily in 3-week-old *rag2*<sup>-/-</sup>  
594 recipient zebrafish treated with DMSO (CTR; n=12, same values as in panels b, c), 20  $\mu$ M  
595 sirolimus (n=12), 20  $\mu$ M everolimus (n=11) or 40  $\mu$ M temsirolimus (n=11) for 6 days. Kaplan-  
596 Meier curves are shown, with statistical analyses performed as in panels B, C. For all experiments  
597 involving drug treatments, drugs were replenished every 2 days during the 6-day course of  
598 treatment (black arrows).

599

600 **Figure 3: Sirolimus, but not trametinib or buparlisib, prevents rapid relapse of *nf1/pten*-**  
601 **mutant melanoma following treatment.** Three-week-old *rag2*<sup>-/-</sup> zebrafish transplanted with  
602 pigmented *nf1/pten*-mutant melanoma cells were treated for 6 days with DMSO, 80 nM  
603 trametinib, 2  $\mu$ M buparlisib, the combination of 80 nM trametinib and 2  $\mu$ M buparlisib, or 20  $\mu$ M  
604 sirolimus. (a, c, e, g, and i) Representative zebrafish at the end of the 6-day drug treatment. (b, d,  
605 f, h, and j) Representative zebrafish at 4 days following the end of drug treatment. (k)  
606 Quantification of melanotic *nf1/pten*-mutant tumor-cell area at the end of the 6-day course of drug  
607 treatment (left), and 4 days later (right). ns p>0.05, \*p<0.05, \*\*p<0.01, \*\*\*p<0.001 by two-tailed,  
608 unpaired t-test. Scale bar = 1mm.

609

610 **Figure 4: Sirolimus strongly inhibits proliferation in *nf1/pten*-mutant melanomas.** (a)  
611 Representative tissue sections from a transplanted *nf1/pten*-mutant melanoma tumor after 2 days  
612 of treatment with DMSO (CTR), 80 nM trametinib, 2  $\mu$ M buparlisib, the combination of 80 nM  
613 trametinib and 2  $\mu$ M buparlisib, or 20  $\mu$ M sirolimus. Sections were immunostained using  
614 antibodies to detect pERK, pAKT, pS6, PCNA, and cleaved caspase-3 (CC3). pERK-, pAKT-

615 and pS6-positive tumor areas, as well as PCNA-positive nuclei, are quantified post-treatment in  
616 panels b-e. “T+B” refers to trametinib plus buparlisib. ns  $p>0.05$ , \*  $p<0.05$ , \*\*  $p<0.01$  by Mann-  
617 Whitney test. Scale bar = 20  $\mu\text{m}$ .

618  
619 **Figure 5: Sirolimus induces a durable cytostatic effect in *nfl/pten*-mutant melanomas.** (a)  
620 Representative tissue sections from a transplanted *nfl/pten*-mutant melanoma tumor at 4 days  
621 after a 6-day drug treatment with DMSO (CTR), 80 nM trametinib, 2  $\mu\text{M}$  buparlisib, the  
622 combination of 80 nM trametinib and 2  $\mu\text{M}$  buparlisib, or 20  $\mu\text{M}$  sirolimus. Sections were  
623 immunostained using antibodies to detect pERK, pAKT, pS6, PCNA, and CC3. pERK-, pAKT-  
624 and pS6-positive tumor areas, as well as PCNA-positive nuclei, are quantified in panels b-e.  
625 “T+B” refers to trametinib plus buparlisib. ns  $p>0.05$ , \*  $p<0.05$ , \*\*  $p<0.01$  by Mann-Whitney  
626 test. Scale bar = 20  $\mu\text{m}$ .

627  
628 **Figure 6: Sirolimus synergizes with venetoclax and S63845 to suppress *nfl/pten*-mutant**  
629 **melanoma tumor growth and extend the survival of tumor-bearing zebrafish.** (a)  
630 Representative sagittal tissue sections from a transplanted *nfl/pten*-mutant melanoma tumor  
631 treated for 2 days with the indicated drugs. Sections were immunostained with antibodies to  
632 detect LC3A/B. *Left panels:* E=eye, B=brain, G=gut, K=kidney, L=liver, S=swim bladder,  
633 T=tumor. *Right panels:* 63X magnification of tumor cells from the small black boxes in left  
634 panels. (b-g) Transplanted *nfl/pten*-mutant melanoma tumor cells were monitored daily in 3-  
635 week-old *rag2*<sup>-/-</sup> recipient zebrafish treated with DMSO (CTR), venetoclax, S63845, sirolimus, or  
636 the drug combinations (n=11 or 12 for each curve; doses as indicated). Kaplan-Meier curves for  
637 PFS (panels b, d and f) and OS (panels c, e and g) were compared using a log-rank test. Drugs  
638 were refreshed every 2 days during the 6-day course of treatment, as indicated by black arrows.  
639 (h) Representative tissue sections from transplanted *nfl/pten*-mutant melanoma tumors treated for

2 days with DMSO (CTR), 7.5  $\mu$ M venetoclax and 2.5  $\mu$ M S63845, 10  $\mu$ M sirolimus, and the three-drug combination. Sections were immunostained using antibodies to detect PCNA and CC3 and quantified in (i). ns  $p>0.05$ , \*\*\* $p<0.0001$  by Mann-Whitney test. Scale bars = 20  $\mu$ m.

**Figure 7: Venetoclax and S63845 synergize with sirolimus to induce apoptosis in human *NF1/PTEN*-deficient melanoma cells.** (a) Western blots for NF1 and PTEN in a panel of human melanoma cell lines. HEK293 and Jurkat cells were included as positive and negative controls. The levels of total ERK1/2 expression serve as the loading control. (b) Relative cell viability of WM-3246 cells (Cell Titer Glo assay) upon treatment with sirolimus, venetoclax or S63845 for 6 days. Mean  $\pm$  s.d. values. (c) Relative cell viability of WM-3246 cells (Cell Titer Glo assay) upon treatment with the combination of sirolimus, venetoclax and S63845 for 6 days. Mean  $\pm$  s.d. values. (d) WM-3246 cell growth kinetics after treatment with the combination of sirolimus, venetoclax and S63845 (for doses see panel c). Mean  $\pm$  s.d. values. (e) Synergistic effects of venetoclax and S63845 on suppression of sirolimus-sensitized WM-3246 cells were analyzed by isobologram analysis. (f) Western blots for BCL2, BCLXL and MCL1 in WM-3246 cells treated with venetoclax or S63845 for 24 hours. (g) Western blots for cleaved caspase-3 in WM-3246 cells treated with the combination of sirolimus, venetoclax and S63845.

**Supplementary Materials**

**Supplementary Figure 1:** Cumulative frequency of tumor development in fish with the indicated genotypes. Malignant peripheral nerve sheath tumors (MPNSTs) comprise the majority of tumors; high grade gliomas are indicated by red arrows with the single black arrow indicating a spontaneous melanoma.

665 **Supplementary Figure 2:** Sections from a spontaneous melanoma from a 20-week-old *nf1a*<sup>+/-</sup>  
666 *;nf1b*<sup>-/-</sup>*;ptena*<sup>+/-</sup>*;ptenb*<sup>-/-</sup>*;p53*<sup>+M214K</sup> zebrafish were stained for H&E, pERK, pAKT, pS6, and  
667 PCNA (63x magnification, Scale bar = 20 μm).

669 **Supplementary Figure 3:** DNA PCR of *nf1a* and *ptena* genes were performed from two pairs of  
670 independent melanoma tumors (T1 and T2) and the corresponding adjacent non-tumor muscle  
671 tissue (A1 and A2). The PCR products were then cut with restriction enzymes that only digests  
672 the wild-type allele but not the mutant allele (DdeI for *nf1a* and RsaI for *ptena*). Electrophoresis  
673 was performed using 3% MetaPhor agarose. The results showed that the wild-type allele of each  
674 gene is retained by the tumor cells.

676 **Supplementary Figure 4:** Amino acid sequence alignment of human and zebrafish BRAF (a) and  
677 NRAS (b). The sites of BRAF codons V600, and NRAS codons G12 and Q61, are highlighted by  
678 red boxes.

680 **Supplementary Figure 5:** Representative sequencing chromatograms of zebrafish codons, shown  
681 are *braf* codon V610, and *nras* codons G12 and Q61 from genomic DNA isolated from a  
682 melanoma tumor (bottom) and matched tumor-free tail fin (top).

684 **Supplementary Figure 6:** Rapid growth of *nf1/pten*-mutant melanoma following intramuscular  
685 engraftment into adult *rag2*<sup>-/-</sup> Casper zebrafish. The implanted melanoma cells (a, indicated by  
686 the arrow) grew aggressively into secondary tumors within 2 weeks (b).

688 **Supplementary Figure 7:** (a) Dose matrices were generated to assess the tolerability of 3-week-  
689 old zebrafish to MEK and PI3K inhibitors. Each matrix sampled mixtures of 2 serially diluted

single-agent concentrations. Three 3-week-old wild-type zebrafish were independently treated with each mixture for 7 days, with drug refreshments at days 2 and 4. The numbers of fish surviving the treatment was measured at the end of day 7. (b) Transplanted *nf1/pten*-mutant melanoma tumor cells were monitored daily in 3-week-old *rag2*<sup>-/-</sup> recipient zebrafish treated with DMSO (CTR; n=12), 1 μM cobimetinib (n=11) and 5 μM apitolisib (n=11) for 20 days. Kaplan-Meier curves for PFS (left) and OS (right) were compared using a log-rank test.

**Supplementary Figure 8:** Transplanted *nf1/pten*-mutant melanoma cells were monitored daily in 3-week-old *rag2*<sup>-/-</sup> recipient zebrafish treated with DMSO (CTR) or selected drugs (n=11 or 12 for each curve). Kaplan-Meier curves for progression-free (left) or overall (right) survival were compared with a log-rank test.

**Supplementary Figure 9:** Transplanted *nf1/pten*-mutant melanoma cells were monitored daily in 3-week-old *rag2*<sup>-/-</sup> recipient zebrafish treated with DMSO (CTR) or selected mTOR inhibitors (n=11 or 12 for each curve). Kaplan-Meier curves for progression-free (left) or overall (right) survival were compared with a log-rank test.

**Supplementary Figure 10:** Transplanted *nf1/pten*-mutant melanoma tumor cells were monitored daily in 3-week-old *rag2*<sup>-/-</sup> recipient zebrafish treated with DMSO (CTR; n=12), 80 nM trametinib (n=11), 2 μM buparlisib (n=12), the combination of 80 nM trametinib and 2 μM buparlisib (n=11), or 20 μM sirolimus (n=12) for 15 days. Kaplan-Meier curves for progression-free (left) or overall (right) survival were compared with a log-rank test (ns p>0.05, \*p<0.05, \*\*p<0.01, \*\*\*p<0.001).

714 **Supplementary Figure 11:** Representative tissue section from a transplanted melanoma tumor  
715 derived from *nf1a*<sup>+/+</sup>;*nf1b*<sup>-/-</sup>;*ptena*<sup>+/+</sup>;*ptenb*<sup>-/-</sup>;*p53*<sup>M214K/M214K</sup>;*Tg(sox10:EGFP)* zebrafish  
716 immunostained with an antibody to GFP. Within the amelanotic tumor mass, a GFP-expressing,  
717 melanin-positive melanoma cell is indicated by the arrow. Scale bar = 20μm.

718  
719 **Supplementary Figure 12: mTOR inhibitors sirolimus and temsirolimus produce a durable**  
720 **antitumor effect on amelanotic *nf1/pten*-mutant melanoma cells.** (a) EGFP-positive  
721 amelanotic melanoma cells were isolated from *nf1a*<sup>+/+</sup>;*nf1b*<sup>-/-</sup>;*ptena*<sup>+/+</sup>;*ptenb*<sup>-/-</sup>  
722 ;*p53*<sup>M214K/M214K</sup>;*sox10:EGFP* zebrafish and injected intraperitoneally into 3-week-old *rag2*<sup>-/-</sup>  
723 zebrafish. Starting at 2 days post-transplantation, the recipient fish were treated with DMSO  
724 (CTR), 80 nM trametinib, 2 μM buparlisib, the combination of 80 nM trametinib and 2 μM  
725 buparlisib, 20 μM sirolimus, or 40 μM temsirolimus for 6 days. EGFP-expressing tumors were  
726 photographed at 4 days post-treatment. The EGFP-expressing area appears as green while the  
727 autofluorescence in the gastrointestinal tract appears as yellow. Scale bar = 1 mm. (b)  
728 Quantification of the area of EGFP tumor fluorescence immediately after the 6-day course of drug  
729 treatment (left) and 4 days later (right). “T+B” refers to trametinib plus buparlisib. ns p>0.05,  
730 \*p<0.05, \*\*p<0.01, \*\*\*p<0.001 by two-tailed unpaired t-test.

731  
732 **Supplementary Figure 13:** Representative tissue sections from a transplanted *nf1/pten*-mutant  
733 melanoma at 4 days after a 6-day drug treatment with DMSO (CTR) and 40 μM temsirolimus.  
734 Sections were immunostained with antibodies to detect pERK, pAKT, pS6, PCNA and CC3.

735  
736 **Supplementary Figure 14:** Dose matrices were generated to assess the tolerability of 3-week-  
737 old zebrafish to sirolimus combined with the indicated drugs. Each matrix sampled mixtures of 2  
738 serially diluted single-agent concentrations. Three 3-week old wild-type zebrafish were

739 independently treated with each mixture for 7 days, with drug replenishment at days 2 and 4. The  
740 numbers of fish surviving the treatment was measured at the end of day 7.

741

742 **Supplementary Figure 15:** Three-week-old *rag2*<sup>-/-</sup> recipient zebrafish were transplanted with  
743 *nfl/pten*-mutant melanoma cells and treated with selected drugs as single agents or in  
744 combination with 5  $\mu$ M sirolimus (n=11 or 12 for each curve). Kaplan-Meier curves for  
745 progression-free (left) or overall (right) survival were compared with a log-rank test. Drugs were  
746 replenished every 2 days during the 6-day course of treatment (black arrows).

747

748 **Supplementary Figure 16:** (a) Venetoclax and S63845 synergize with sirolimus to suppress  
749 human melanoma cells harboring BRAFV600E and PTEN mutations. Relative cell viability of  
750 COLO829 and C32 cells (Cell Titer Glo assay) upon treatment with the combination of sirolimus,  
751 venetoclax and S63845 for 3 days. Mean  $\pm$  s.d. values. (b) Venetoclax and S63845 synergize  
752 with dabrafenib to kill BRAF-mutant melanoma cells. Relative cell viability of C32 cells (Cell  
753 Titer Glo assay) upon treatment with the combination of dabrafenib, venetoclax and S63845 for 3  
754 days. Mean  $\pm$  s.d. values.

755

756 **Supplementary Material and Methods**

757  
758 **DNA extraction, PCR and sequencing**

759 From each *nf1a*<sup>+/-</sup>;*nf1b*<sup>-/-</sup>;*ptena*<sup>+/-</sup>;*ptenb*<sup>-/-</sup>;*p53*<sup>M214K/M214K</sup> fish, the melanoma tumor and the tumor-  
760 free tail fin were excised, and genomic DNA was extracted with 30 µL QuickExtract DNA  
761 Extraction Solution (Epicentre, Madison, WI) according to the manufacturer's instructions. PCR  
762 reactions were performed in a 25 µL volume consisting of 4 µL genomic DNA, 1.4 µL 2.5 mM  
763 dNTP (Invitrogen, Carlsbad, CA), 0.16 µL SuperTaq enzyme (NEB, New England Biolabs,  
764 Ipswich, MA), 2.5 µL 10x SuperTaq buffer (NEB) and 1.4 µL 10 µM primer mix. Cycling  
765 parameters were 1) 94°C for 2 min, 2) 40 cycles at 94°C for 30 sec, annealing (temperature  
766 depends on primer sets, see below) for 30 sec, and elongation at 72°C for 30 sec, and 3) final  
767 elongation for 5 min at 72°C. PCR primer sequences and annealing temperatures were as follow:  
768 *nf1a* forward, 5'-GGTGTGTATGTAAATGGGCTCAATG-3' and reverse 5'-  
769 TACAGTTTCCATAAAACCTGACATTTC-3' (62°C); *ptena* forward, 5'-  
770 TTGCCATGGGCTTTCCAGCCGTA-3' and reverse 5'-  
771 CCACGTTGACTTACCGGACAACGTCA-3' (53°C); *brafV610* forward, 5'-  
772 ATTAGCCGTAACATCACTTCTCTAG-3' and reverse 5'-  
773 ATGTAAGATGTGTTCCTTCACTCAC-3' (53°C); *nrasG12* forward, 5'-  
774 GCTTACTCTCTGTCTTTAATTAC-3' and reverse 5'- AAGTATAGTAAATTTCTCAT-3'  
775 (53°C); *nrasQ61* forward, 5'-GTGGCAATCTTGTCTTTTC-3' and reverse 5'-  
776 CTGCTCTCAGACCTGTAC-3' (60°C). Sequencing of the PCR reaction products were  
777 performed by Genewiz (Cambridge, MA).

778  
779 **Immunohistochemistry**



780 Zebrafish were euthanized in tricaine anesthetic, fixed in 4% paraformaldehyde at 4°C for 2 days,  
781 and decalcified with 0.25 M EDTA, pH 8.0, for at least 24 hr. Paraffin sectioning followed by  
782 H&E staining or IHC was performed at the Dana-Farber/Harvard Cancer Center Research  
783 Pathology Core. Primary antibodies included phospho-p44/42 MAPK (ERK1/2) (Thr202/Tyr204,  
784 Cell Signaling #4370; 1:150), phospho-AKT (Ser473, Cell Signaling #4060), phospho-S6  
785 ribosomal protein (Ser240/244, Cell Signaling #4838), PCNA (PC10, EMD Millipore; 1:100),  
786 cleaved caspase-3 (Cell Signaling #9664; 1:100), GFP (Abcam #6556, 1:150), LC3A/B (Cell  
787 Signaling #12741; 1:200), HSP90 (Cell Signaling #4874; 1:100), and HSP70 (Enzo #ADI-SPA-  
788 810; 1:25). Antibody binding was detected with either a diaminobenzidine-peroxidase (DAB)  
789 visualization system (EnVision+, Dako, Carpinteria, CA) or a Bond Polymer Refine Red  
790 Detection Kit (Leica Biosystems, Buffalo Grove, IL). Mayer's hematoxylin was used for  
791 counterstaining.

792

793 **Imaging and quantification**

794 For brightfield DIC images, a Zeiss Axio Imager.Z1 compound microscope equipped with an  
795 AxioCam HRc was used. For live imaging, zebrafish were anaesthetized using 0.016% tricaine  
796 (Sigma) and mounted in 3% methylcellulose (Sigma). A Nikon SMZ1500 microscope equipped  
797 with a Nikon digital sight DS-U1 camera was used for capturing both the brightfield and  
798 fluorescent images from live zebrafish. For melanoma quantification, all animals in the same  
799 experiments were imaged under the same conditions, and the acquired fluorescent images were  
800 quantified using the ImageJ software by measuring the pigment or EGFP fluorescence. The  
801 pigment or fluorescent area was normalized against the surface area of the fish head to control for  
802 varying size of fish. Overlays were created using ImageJ and Adobe Photoshop 7.0.1.

803

804 **Drug treatment**

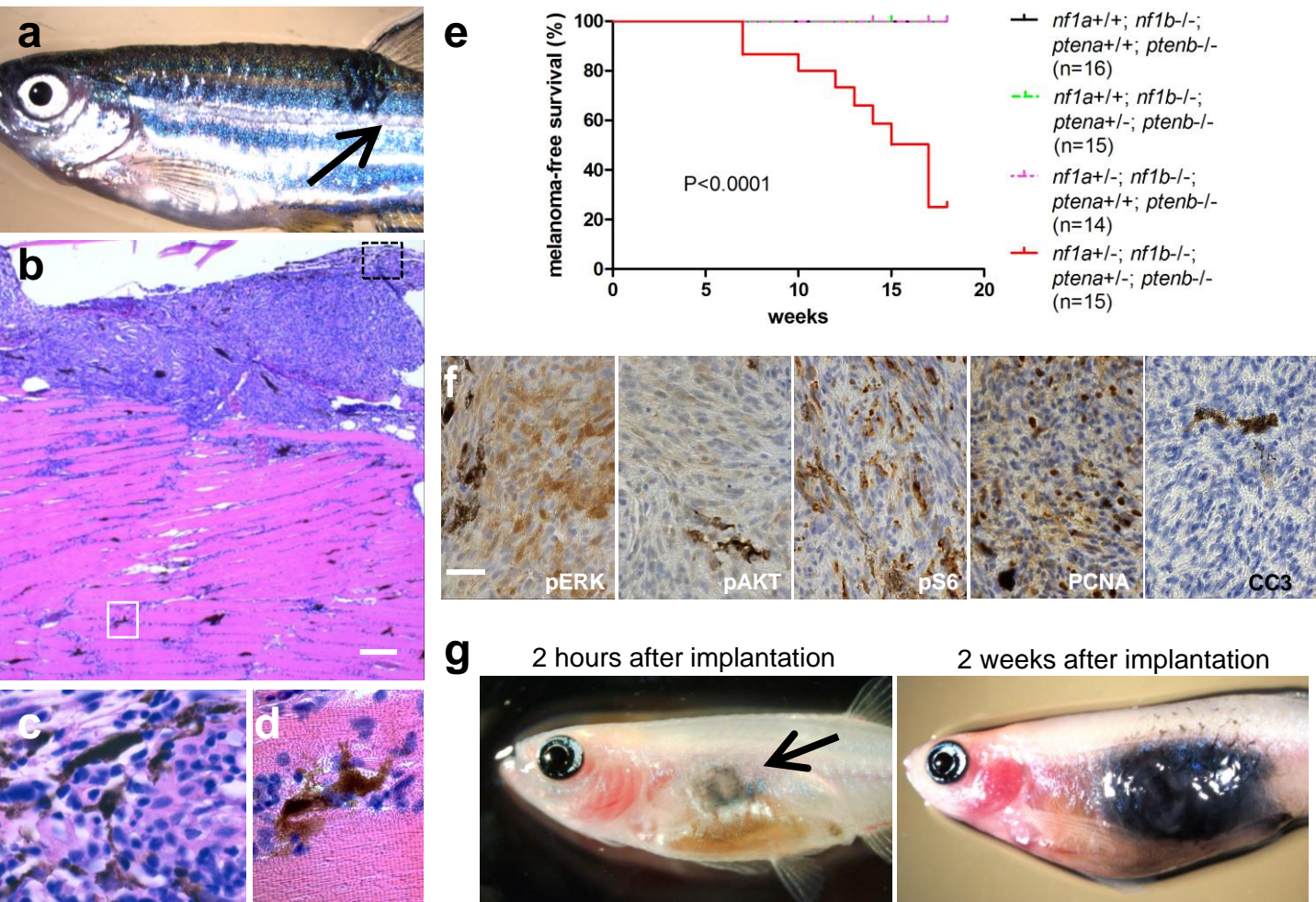
805 After 2 days of post-transplantation recovery, the 3-week-old juvenile *rag2*<sup>-/-</sup> fish transplanted  
806 with *nfl/pten*-mutant melanoma cells were randomly separated and treated with trametinib  
807 (Selleck Chemicals, Houston, TX), cobimetinib (Selleck), buparlisib (Selleck), apitolisib  
808 (Selleck), sirolimus (rapamycin, LC Laboratories, Woburn, MA), everolimus (LC Laboratories),  
809 temsirolimus (LC Laboratories), sorafenib (LC laboratories), sabutoclax (Selleck), obatoclax  
810 (Santa Cruz), chloroquine (Sigma), olaparib (Selleck), venetoclax (Chemietek, Indianapolis, IN)  
811 and S63845 (Chemgood, Glen Allen, VA) with refreshment every 2 days. Sample size was  
812 estimated according to [https://www.statstodo.com/SSizSurvival\\_Pgm.php](https://www.statstodo.com/SSizSurvival_Pgm.php), that with at least 10  
813 animal per group, we will have 90% power to identify 20% tumor suppression, or 95% power to  
814 identify 50% tumor suppression, testing at the 0.05 one sided level using a log-rank test. The  
815 drug treatment experiments were all blinded that the drug administration and tumor progression  
816 monitoring were performed by independent investigators. The treatment conditions were  
817 unblinded after the completion of tumor monitoring. Each experiment was replicated at least  
818 three times in the laboratory.

819

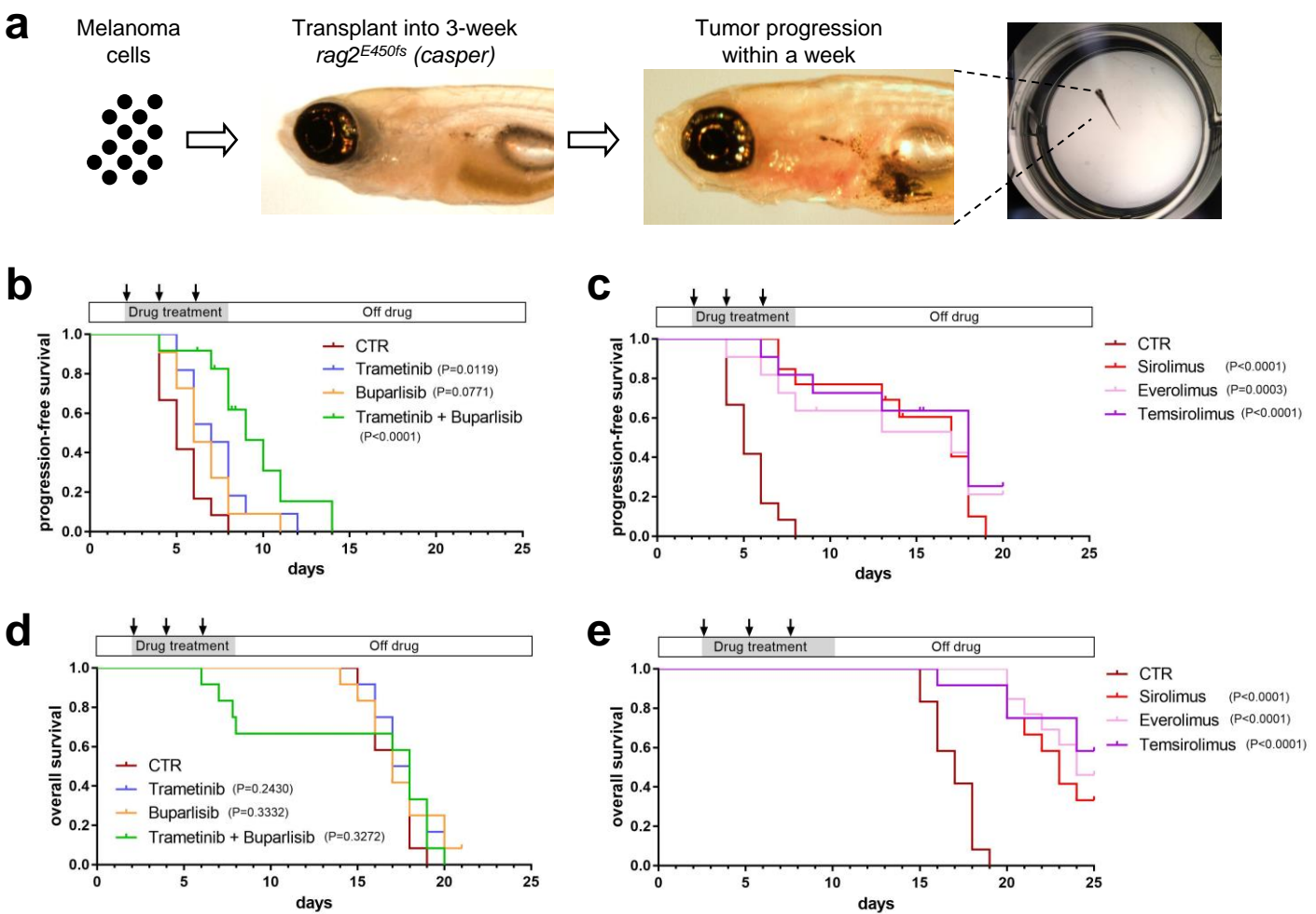
820 **Western blots and antibodies**

821 Whole-cell lysates were prepared in RIPA buffer. Protein concentration was quantified with a  
822 Pierce BCA Protein Assay Kit (Thermo Fisher Scientific Inc.). Equivalent amounts of protein  
823 were diluted in the Laemmli samples buffer (Bio-Rad Laboratories) and separated by SDS-PAGE.  
824 Proteins were transferred to PVDF membranes (Millipore, Billerica, MA) and subjected to  
825 immune blot analysis with each of the specific antibodies for NF1 (Bethyl Laboratories #A300-  
826 140A-M; 1:2000 dilution), PTEN (Cell Signaling #9188; 1:1000 dilution), total ERK1/2 (Cell  
827 Signaling #4695; 1:1000 dilution), and cleaved caspase 3 (Cell Signaling #9661; 1:500 dilution).  
828 All primary antibodies were diluted in 5% milk in PBST (0.5% Tween-20 in PBS).

He *et al*, Figure 1



# He et al, Figure 2





**CTR**

# Trametinib

## Buparlisib

## Trametinib + Buparlisib

## Sirolimus

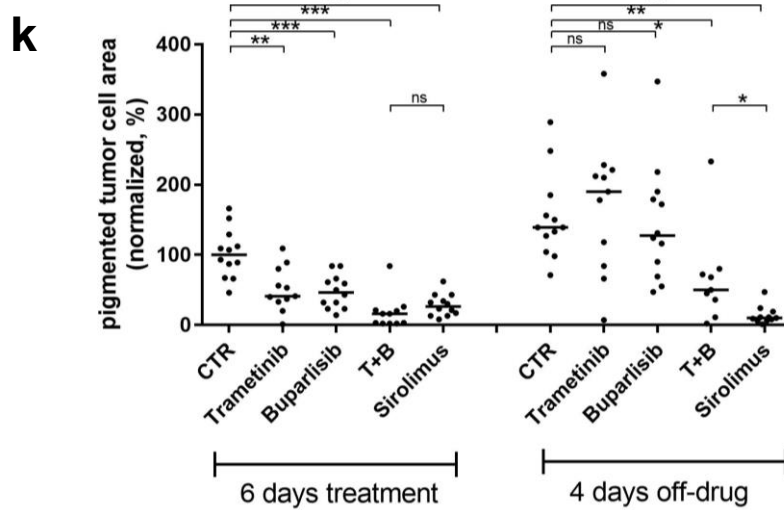
**b**

**d**

**f**

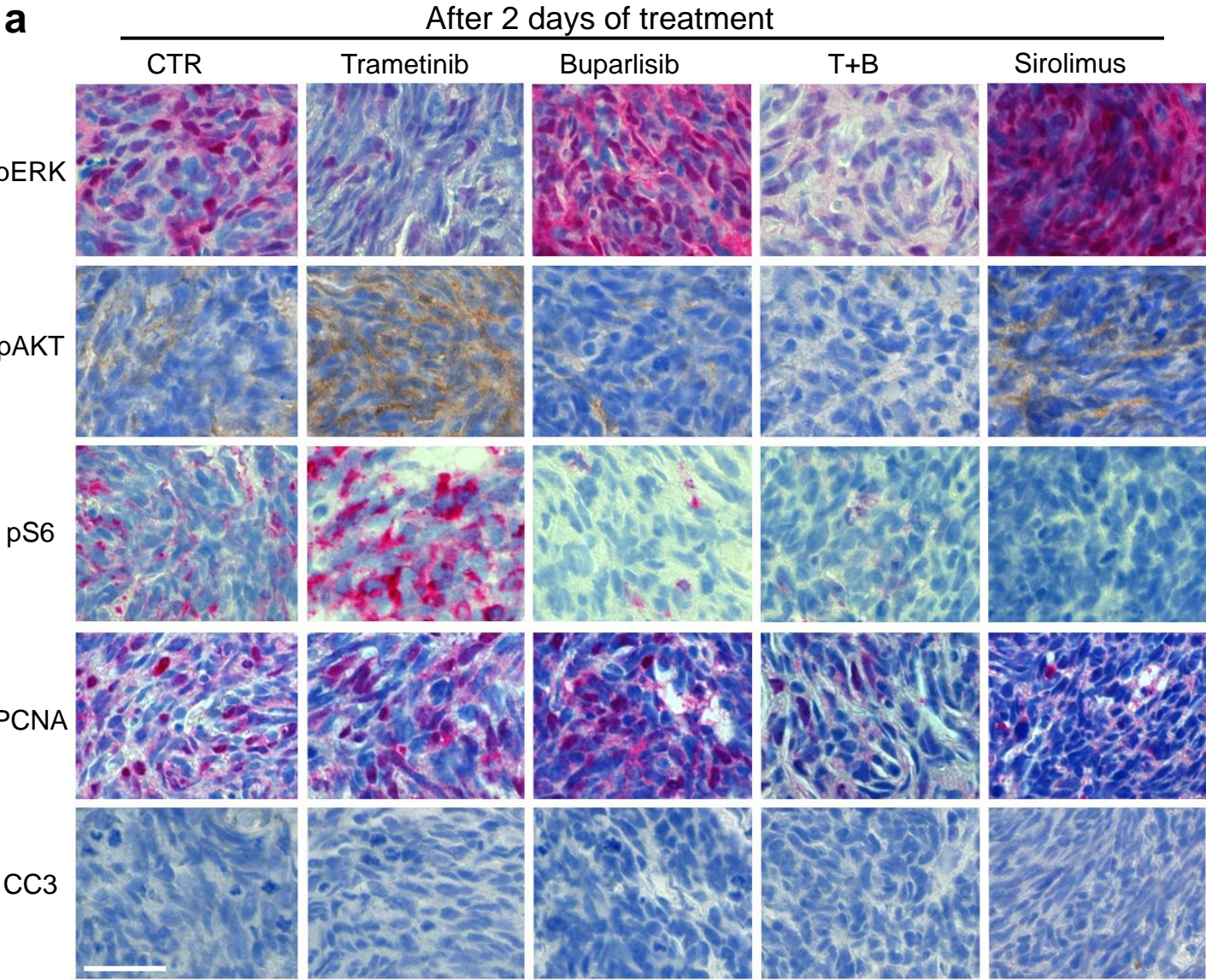
# h

j

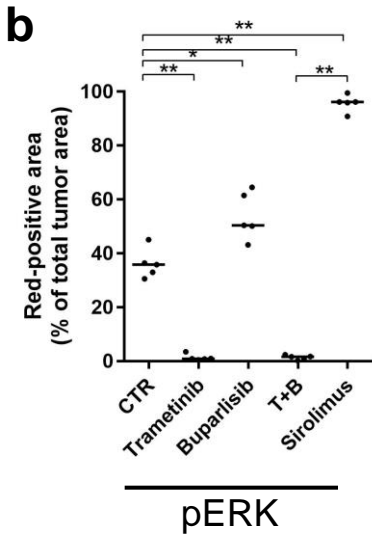




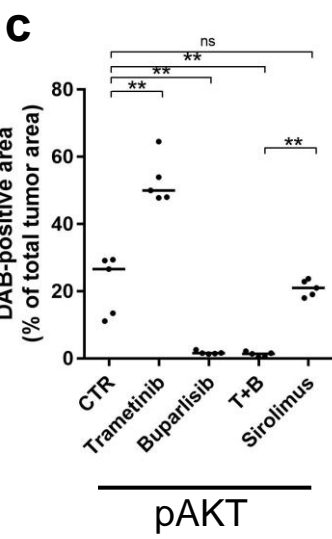
**a**



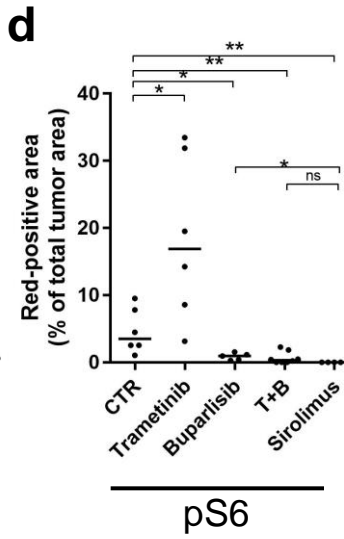
**b**



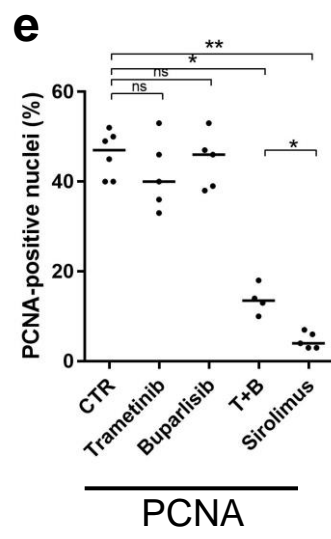
**c**



**d**

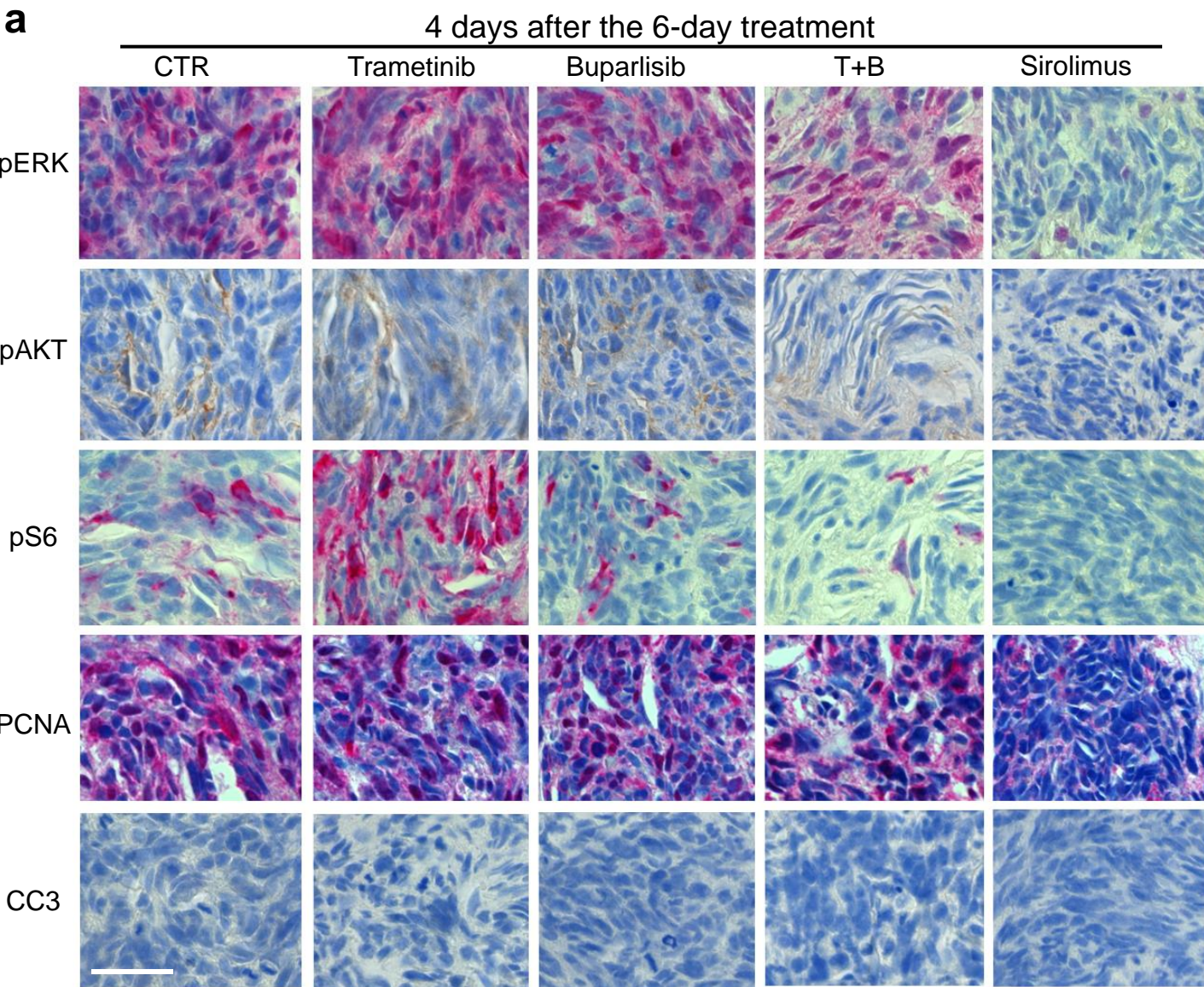


**e**

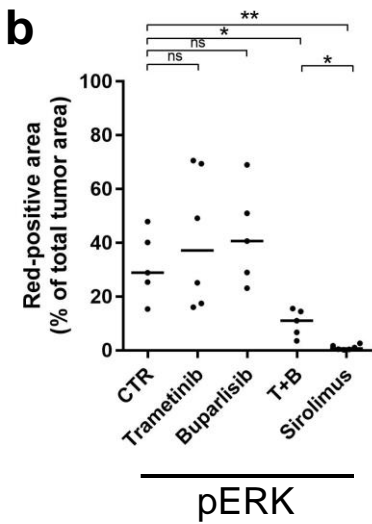




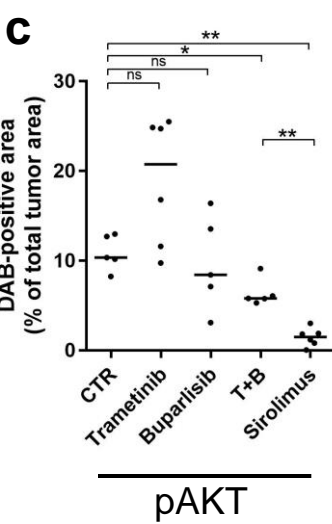
**a**



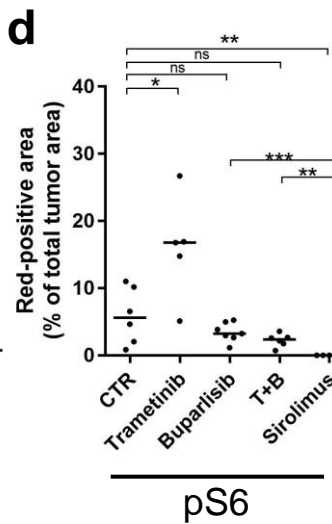
**b**



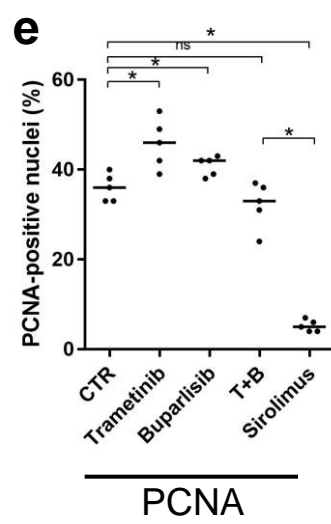
**c**

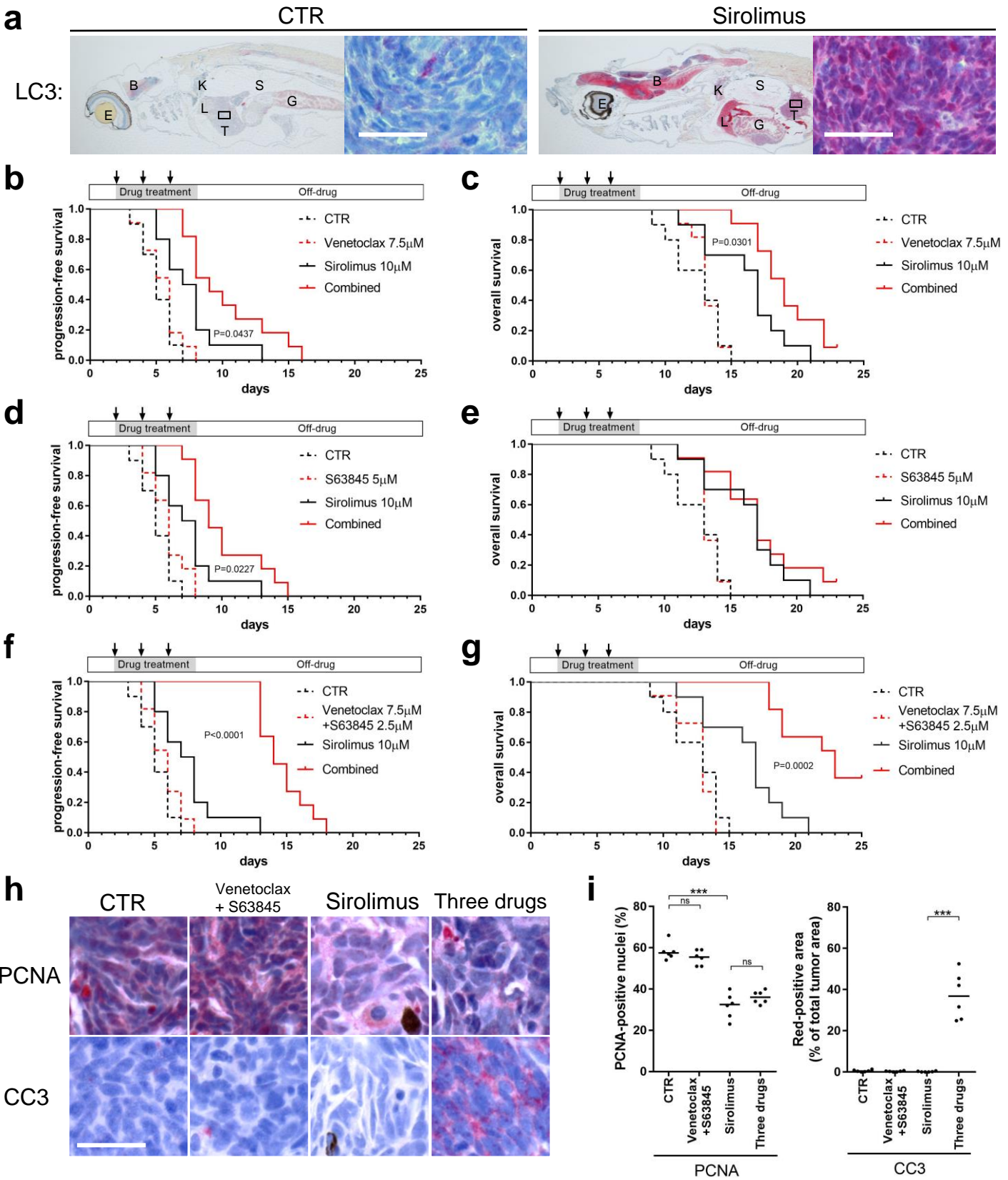


**d**



**e**

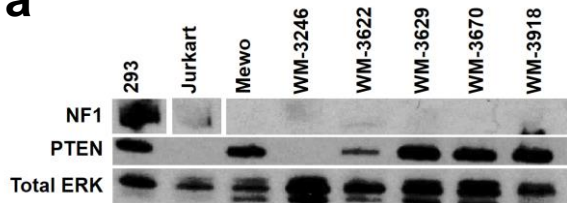




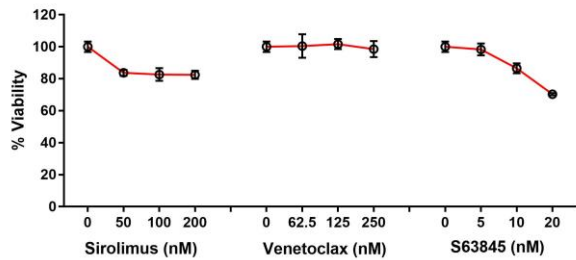


He *et al*, Figure 7

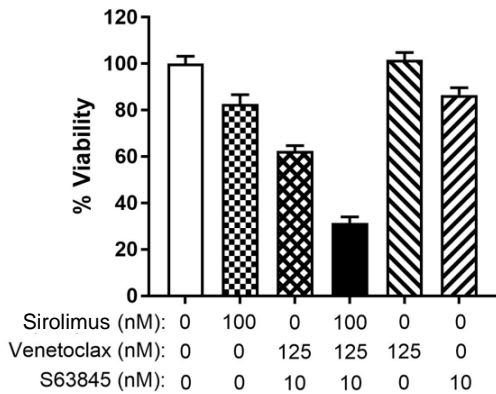
**a**



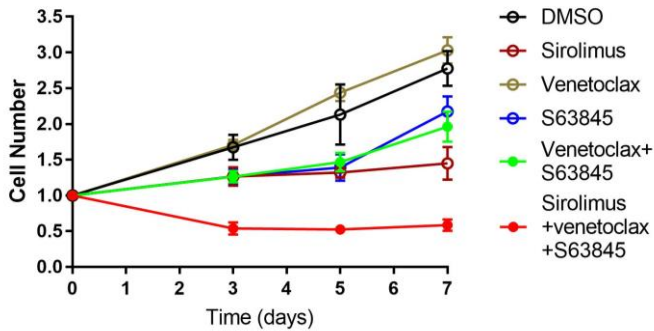
**b**



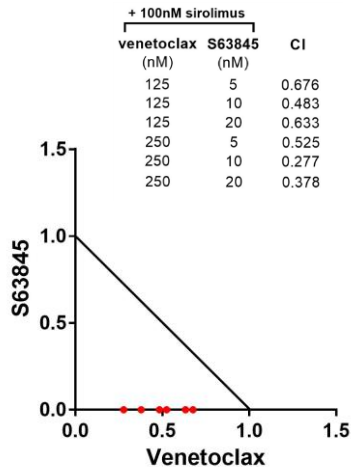
**c**



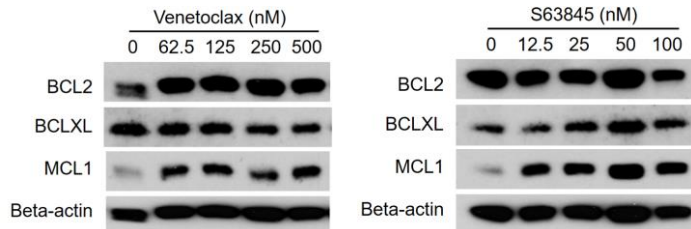
**d**



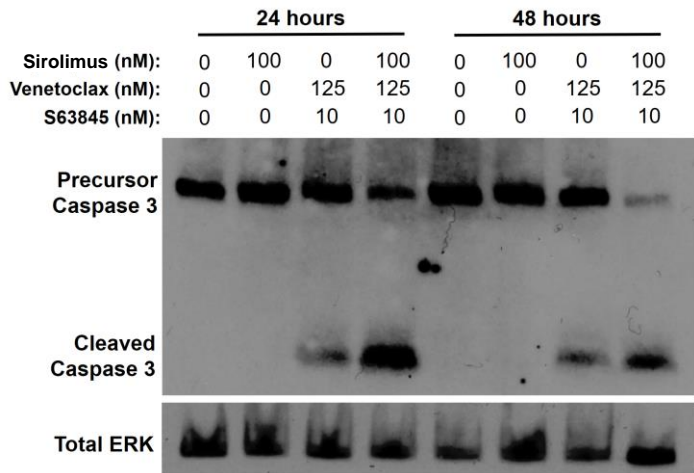
**e**



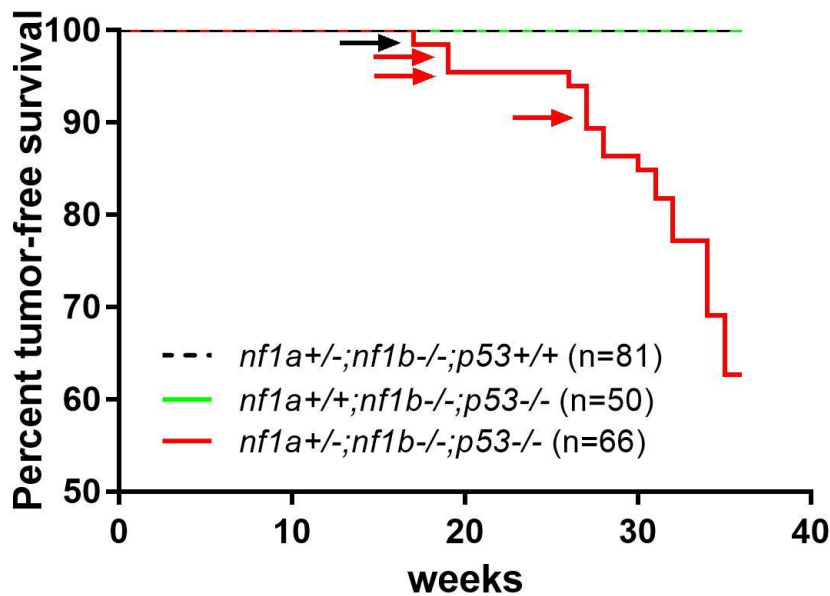
**f**



**g**



He *et al*, Supplementary Figure 1



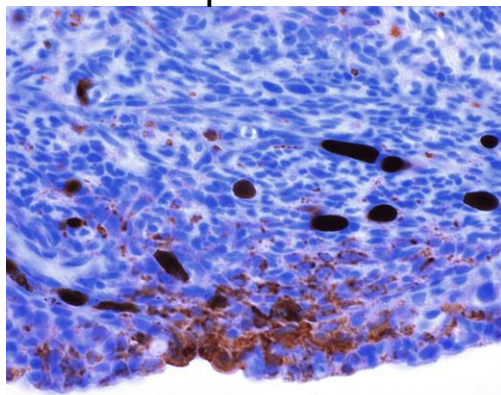
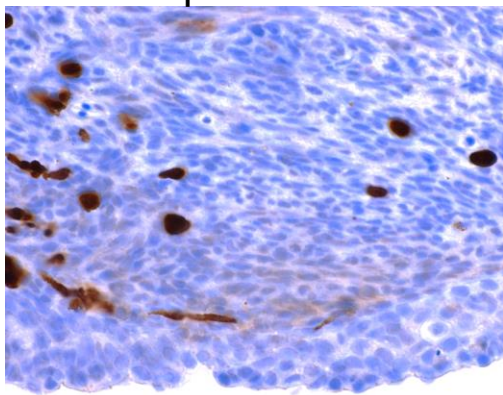
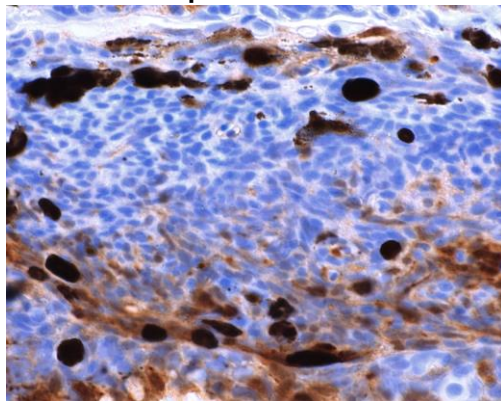
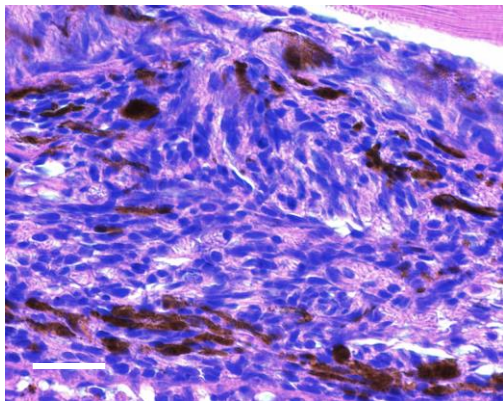
He *et al*, Supplementary Figure 2

HE

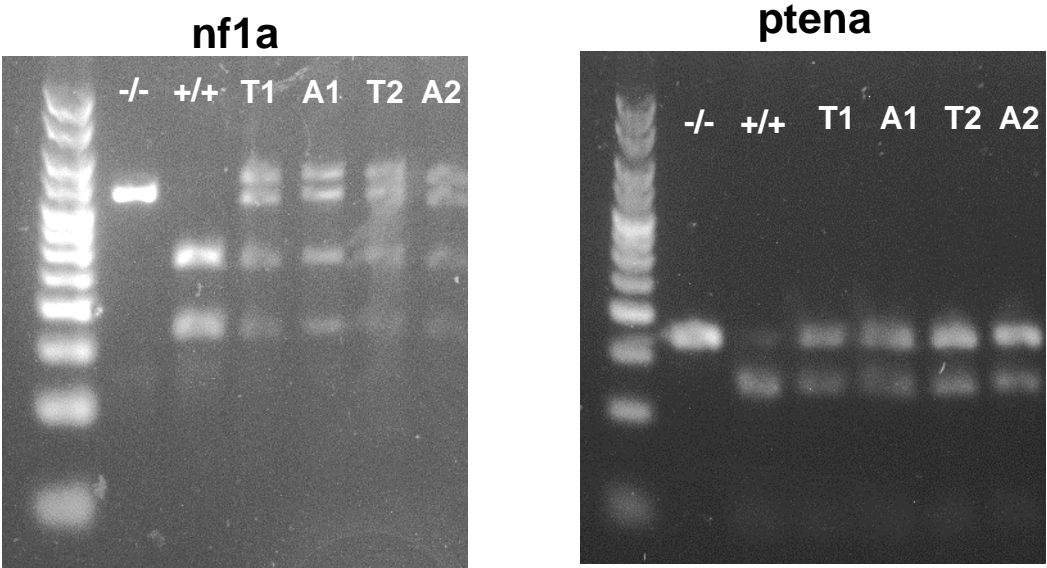
pERK

pAKT

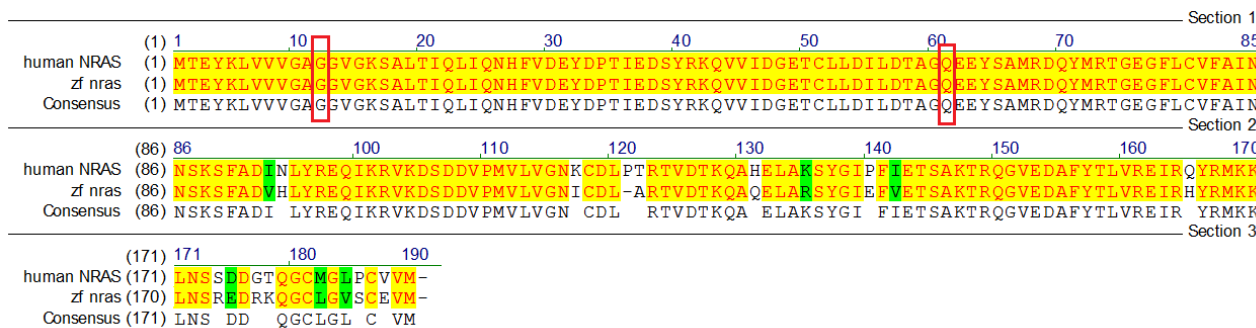
pS6



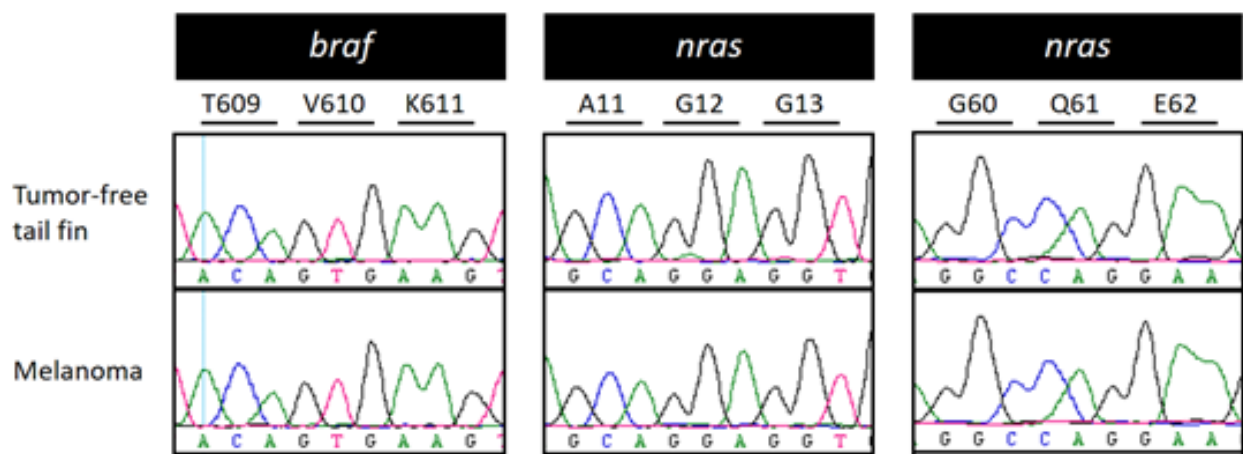
He *et al*, Supplementary Figure 3



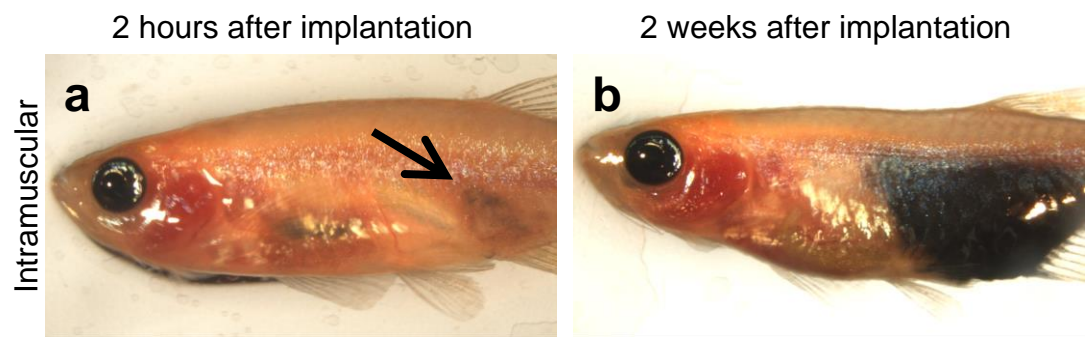
a



He *et al*, Supplementary Figure 5



He *et al*, Supplementary Figure 6



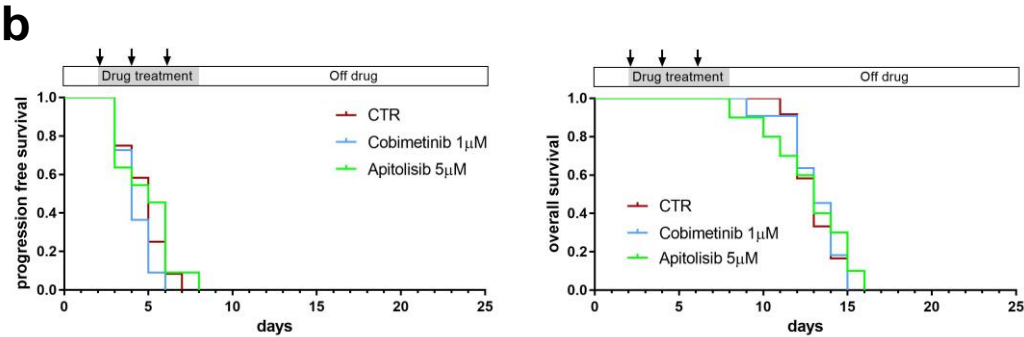


# He *et al*, Supplementary Figure 7

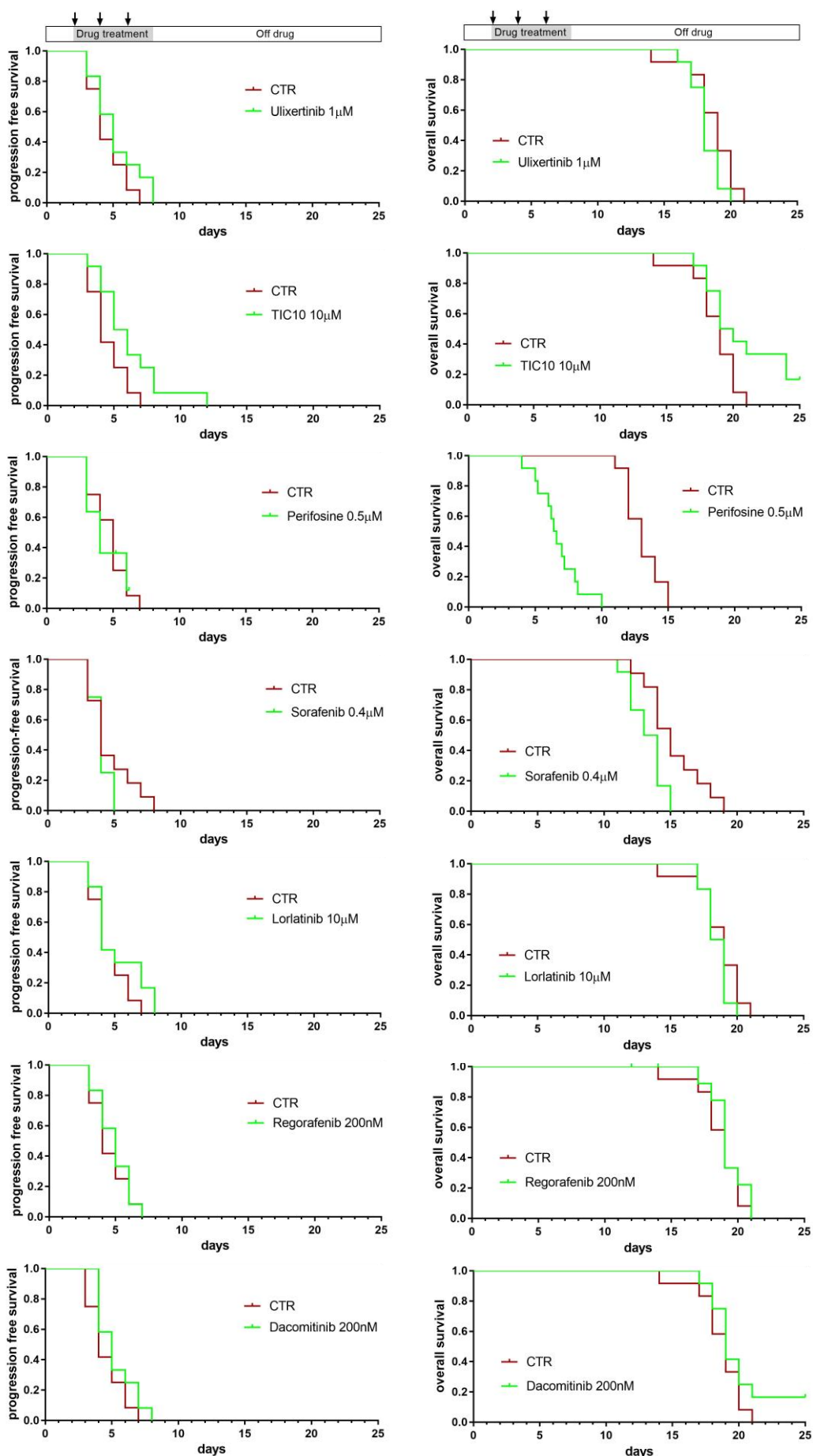
**a**

Trametinib (nM)	
	0   20   40   80   100
Buparlisib (μM)	
0	3   3   3   3   0
0.5	3   3   3   3   -
1	3   3   3   3   -
2	3   3   3   3   -
4	0   -   -   -   -

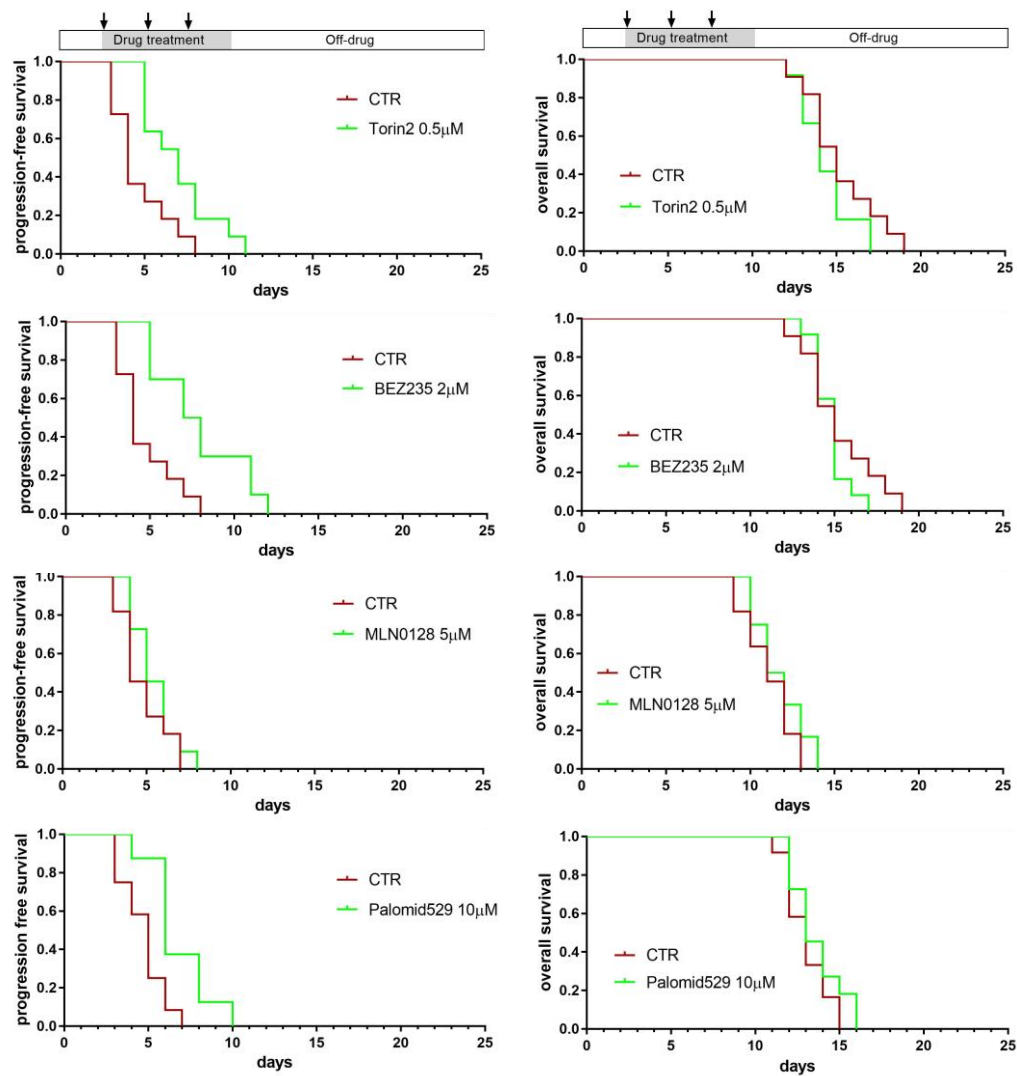
Cobimetinib (μM)	
	0   0.2   0.5   1   2   5
Apitolisib (μM)	
0	3   3   3   3   2   0
1	3   3   1   0   0   -
2	3   2   0   0   0   -
5	3   0   0   0   0   -
10	0   -   -   -   -   -



He *et al*,  
Supple  
mentary  
Figure 8

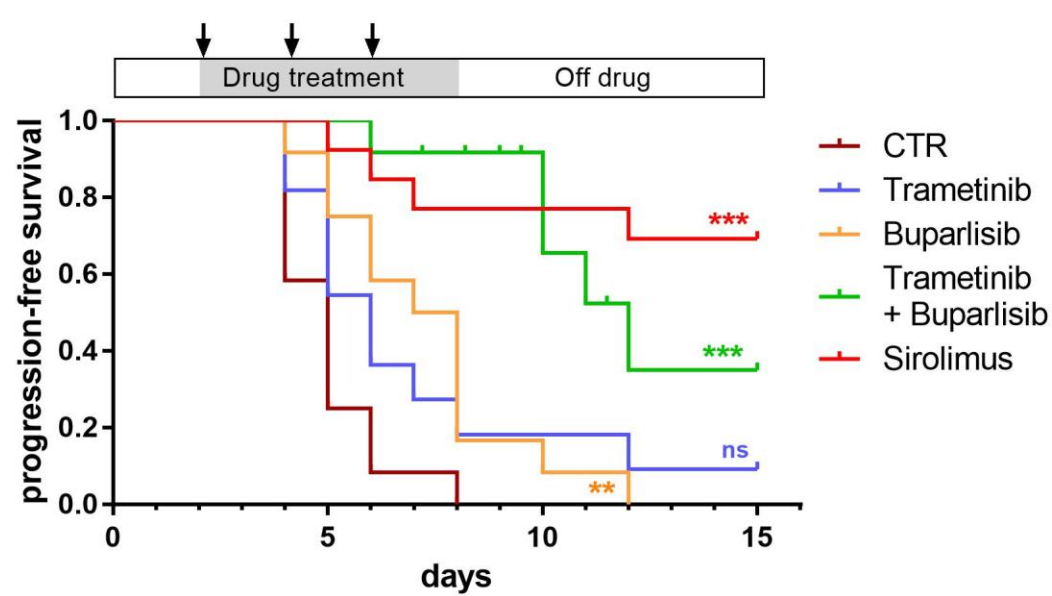


# He et al, Supplementary Figure 9

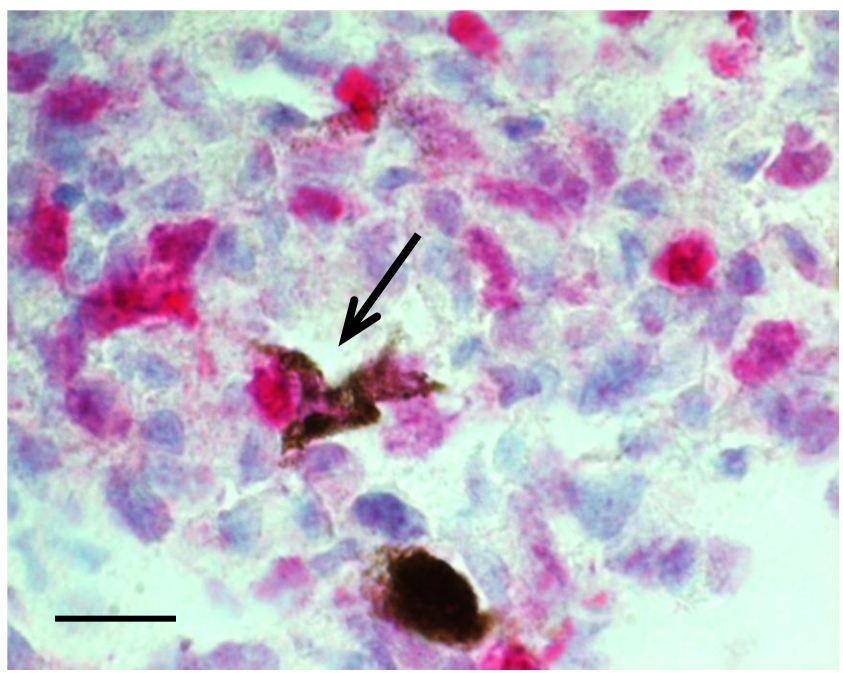


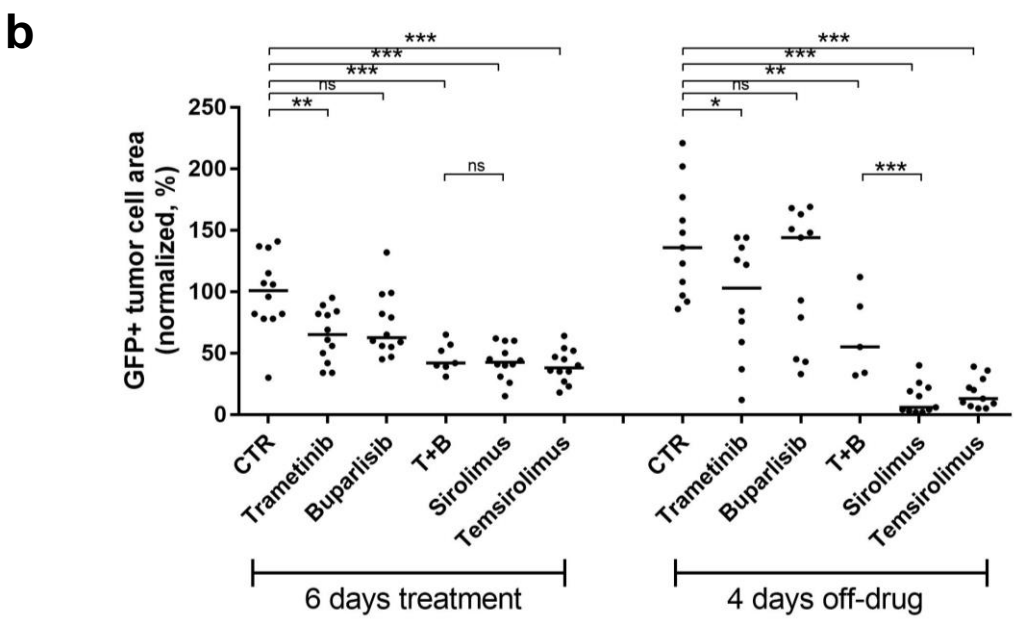
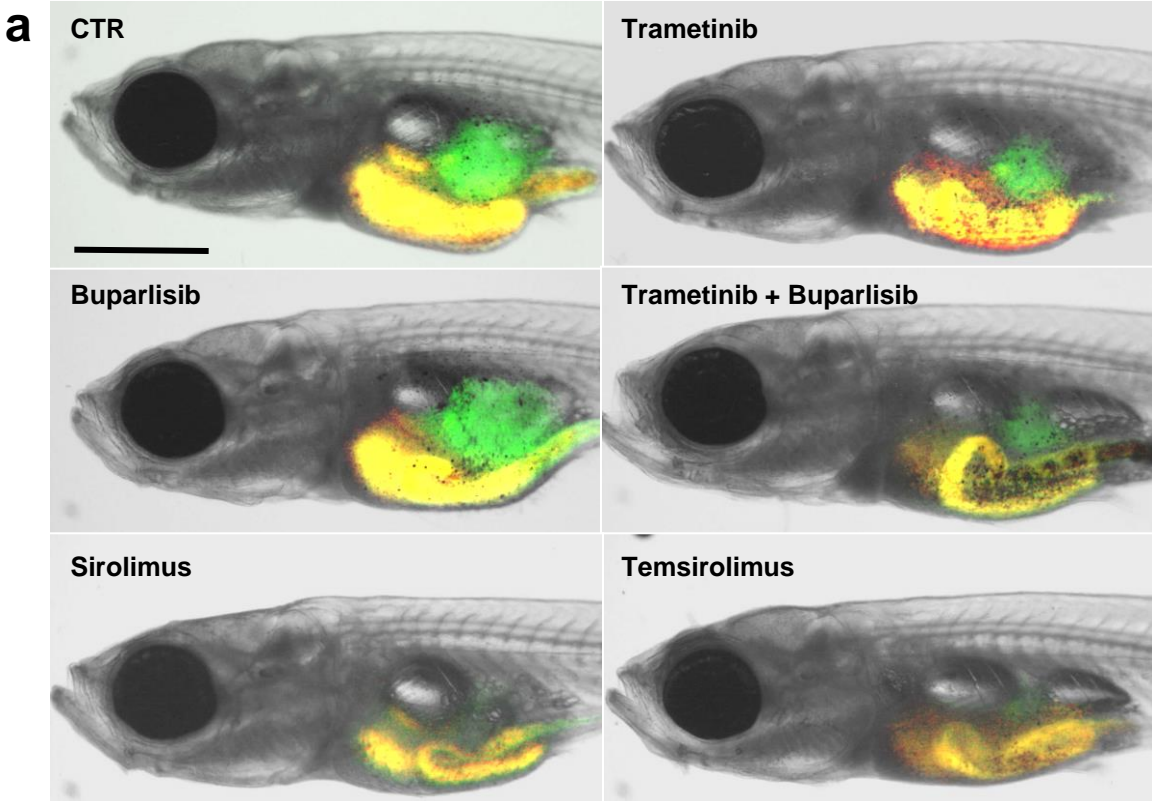


He *et al*, Supplementary Figure 10

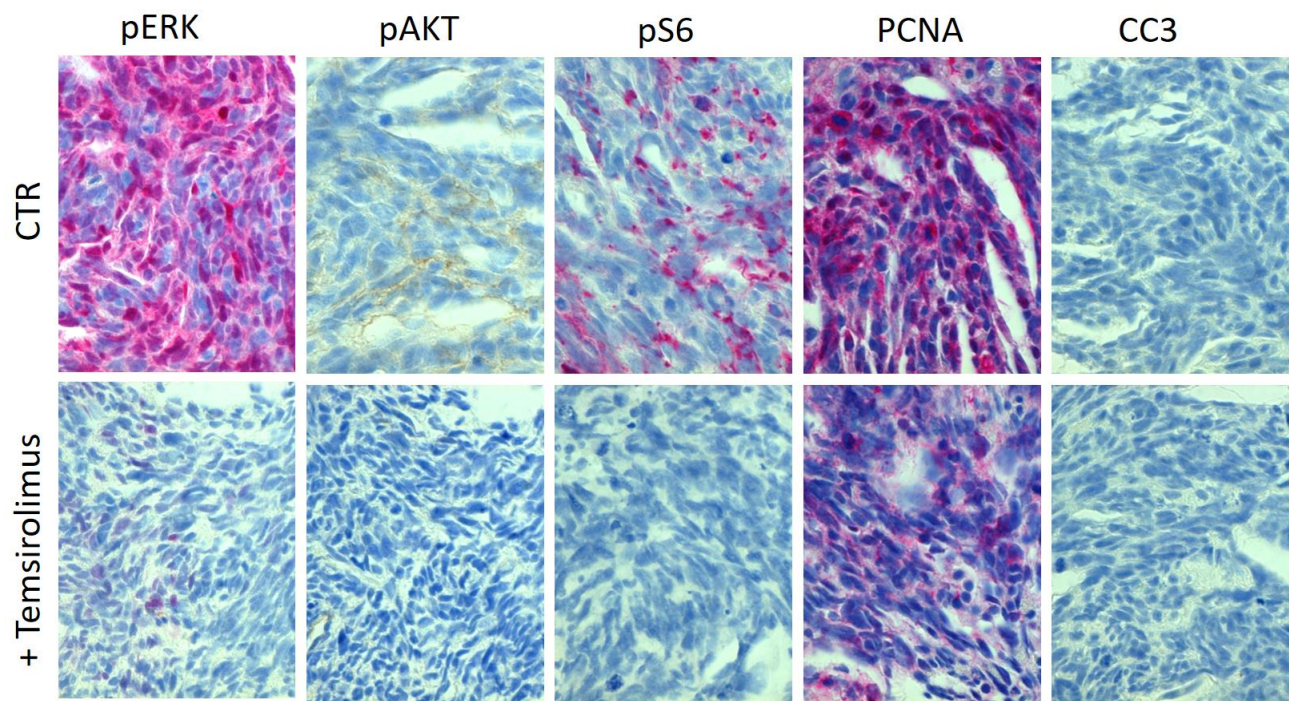


He *et al*, Supplementary Figure 11



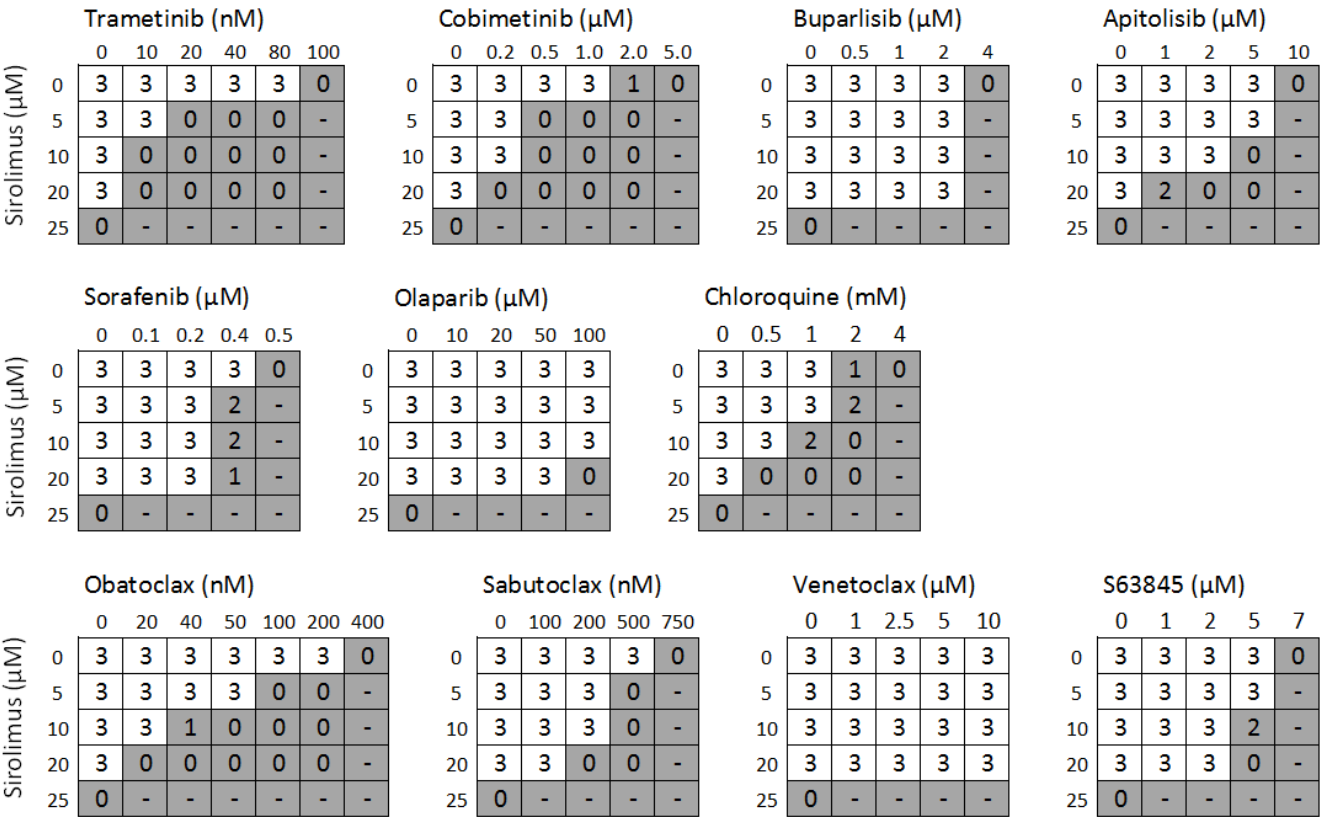


He *et al*, Supplementary Figure 13

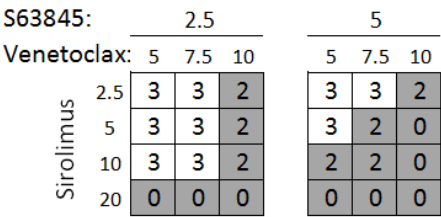


# He et al, Supplementary Figure 14

## Two drug combinations:



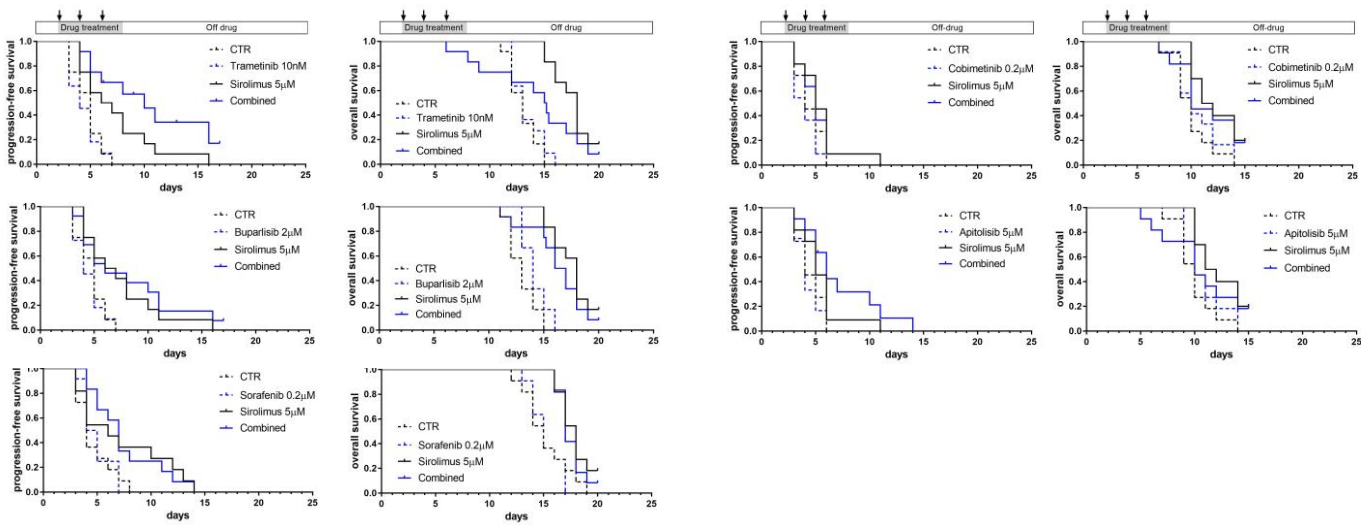
## Three drug combination:



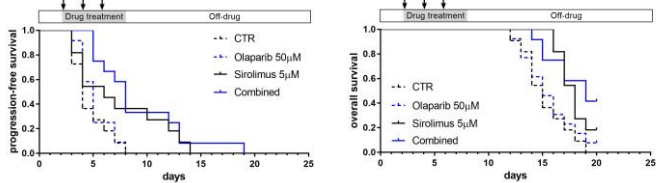


# He *et al*, Supplementary Figure 15

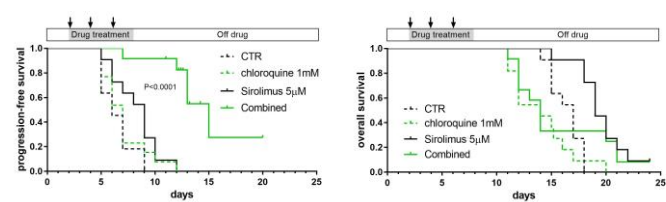
## Kinase inhibitors



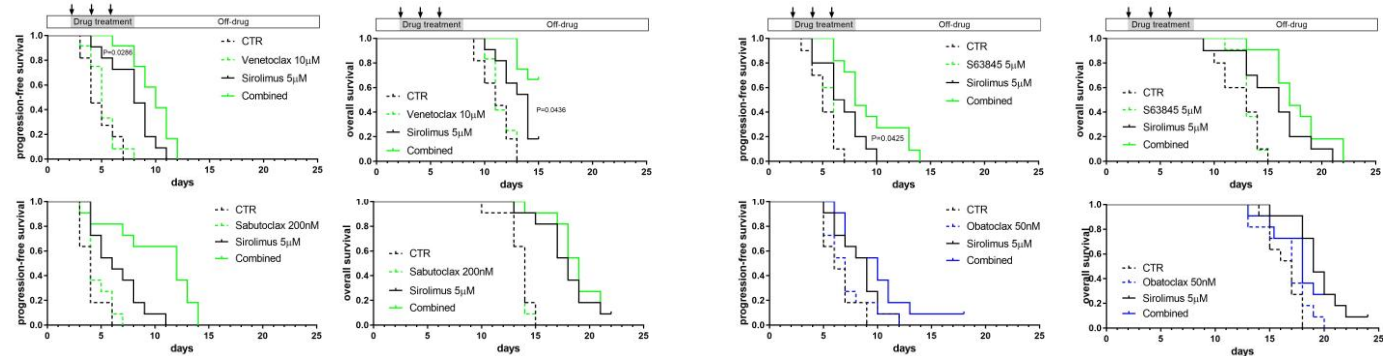
## PARP1 inhibitor



## Autophagy inhibitor

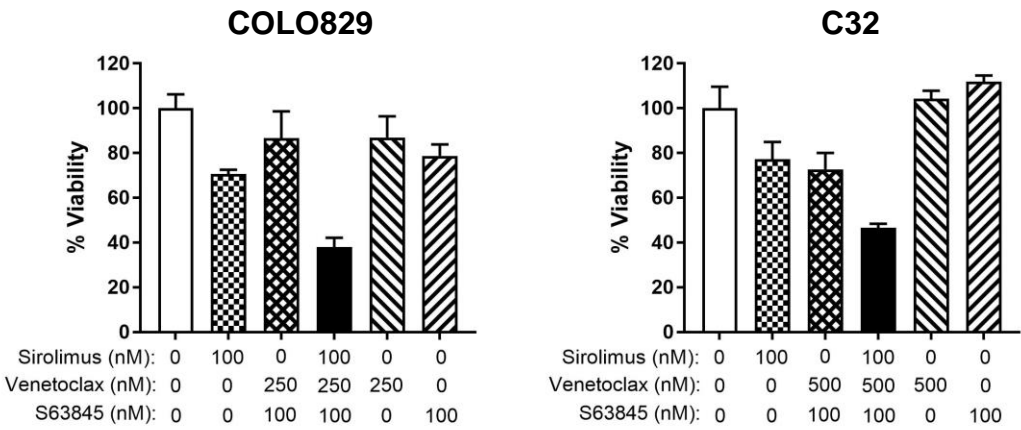


## Inhibitors against BCL2-family of prosurvival proteins



He et al, Supplementary Figure 16

a



b

